UNIVERSIDADE DA BEIRA INTERIOR

Ciências

Novas abordagens terapêuticas para a regeneração óssea

João Miguel Carvalho Freire Boga

Dissertação para obtenção do Grau de Mestre em

Biotecnologia

(2º ciclo de estudos)

Orientador: Professor Doutor Ilídio Joaquim Sobreira Correia

Co-orientador: Mestre Sónia Alexandra Pereira Miguel

Covilhã, outubro de 2017

"See that the imagination of nature is far, far greater than the imagination of man."
Richard P. Feynman

Dedicado, à minha querida família, com muito amor e carinho.

Acknowledgments

First of all, I would like to thank my supervisor Professor Ilídio Correia for the chance to pursue the topic of my masters' thesis with him. For all his commitment and time spent in carrying out this project in its entirety.

To my co-supervisor, Sónia Miguel for her unwavering support both as an academic, in acquiring scanning electron microscopic images and helping me throughout my entire thesis, as well as being a good friend, always there when I needed her the most.

To Professor Abílio Silva, for his availability and the assistance provided in the mechanical characterization of the scaffolds.

To Duarte, for providing me the Graphene Oxide material, for helping me brainstorm ideas and teaching me the importance of scientific rigor.

To my colleagues, I'd like to thank Elisabete for all the moments and conversations that we had the opportunity to share, André for his challenging insights, and his willingness to lend me a hand whenever needed and Sergio for the steady stream of jokes to keep me going. Thank you all!

To Duarte Nuno, for all the hours and days that you had to endure without me being there, or just being too busy to be there to share awesome moments. To João Duarte I would like to thank for the arguments that we had and for all the moments, be it in classes or over a coffee.

To my friends, for the unconditional attention and support, that you guys offered whenever I had a rough day.

And finally, but not least, to my family whose extraordinary support got me through all of this, be it on the sunniest of days or the darkest of nights, for all their love, understanding and words of advice that they gave me during the course of all these years!

Resumo

O envelhecimento da população mundial tem associado um aumento do número de doenças e fraturas ósseas, as quais comprometem a integridade do osso e afetam a qualidade de vida dos indivíduos. Na atualidade, estes tipos de desordens são tratadas recorrendo aos enxertos ósseos, nomeadamente aos autoenxertos. Contudo estes tipos de enxertos têm limitações como seja a disponibilidade do enxerto, possibilidade de induzir dor crónica ou ainda ser rejeitado devido a contaminação bacteriana no decorrer da cirurgia. Neste contexto, têm sido desenvolvidas novas abordagens terapêuticas com o intuito de colmatar as limitações associadas aos tratamentos usados comumente na clínica. Uma das abordagens usadas consiste na produção de estruturas tridimensionais (*scaffolds*) capazes de mimetizar as propriedades mecânicas e biológicas do osso nativo. Para este fim, neste estudo foram desenhados *scaffolds* cilíndricos, usando design assistido por computador, com o intuito de mimetizar a geometria natural dos ossos ocos e permitir a troca de nutrientes e a neovascularização.

No presente estudo os *scaffolds* foram produzidos recorrendo a fosfato tricálcico, ácido algínico e óxido de grafeno (GO) usando uma Fab@home *3D-Plotter*. As propriedades mecânicas e biológicas das estruturas tridimensionais foram caracterizadas através de diversas técnicas. Os resultados obtidos neste estudo demonstraram que as amostras contendo GO possuem maior porosidade, mantendo, no entanto, constante a sua resistência mecânica. Adicionalmente, os *scaffolds* 60/40_GO revelaram uma maior capacidade para fixar cálcio e fósforo na sua superfície, o que contribui para melhorar a sua osteoinductividade e osteoconductividade. Propriedades estas que são essenciais para a osteointegração do *scaffold*. Os resultados obtidos neste projeto demonstraram que os *scaffolds* funcionalizados com GO possuem as propriedades requeridas para a sua aplicação na regeneração óssea.

Palavras-chave

Engenharia de Tecido Ósseo; Impressão 3D; Óxido de Grafeno; Prototipagem Rápida; *Scaffolds* 3D biocompósitos;

Resumo Alargado

O osso é um tecido extremamente dinâmico e vascularizado, que está envolvido em diferentes funções tais como: locomoção, proteção dos órgãos contra ameaças externas e armazenamento de minerais essenciais à homeostase do corpo humano. A matriz óssea é constituída por um bio-compósito dotado de uma fase orgânica (maioritariamente colagénio tipo I) e uma fase inorgânica (hidroxiapatita) assim como uma componente celular (osteoblastos, osteócitos e osteoclastos) e água. Este tecido possui também uma capacidade inata de auto-regeneração que permite ao sistema esquelético responder a estímulos exteriores e reparar possíveis danos estruturais. Contudo em certas situações esta capacidade regenerativa é comprometida, nomeadamente em defeitos ósseos extensos, envelhecimento e em certas doenças que tornam a osso propenso a fraturas. Na clínica os autoenxertos, aloenxertos e xenoenxertos têm sido usados para tratar fraturas que afetam este tecido. Contudo, estas abordagens terapêuticas possuem certas desvantagens que incluem uma limitada disponibilidade dos autoenxertos, a rejeição ou infeção bacteriana que por vezes surge quando são usados alo ou xenoenxertos. Com o intuito de ultrapassar estas limitações, os investigadores da área de Engenharia de Tecidos têm vindo a desenvolver novas abordagens terapêuticas que procuram acelerar o processo regenerativo do osso. Na atualidade têm sido produzidas novas matrizes tridimensionais que procuram mimetizar tanto a estrutura como a composição do tecido nativo de forma a restaurar, manter ou melhorar a função do tecido danificado. Estas estruturas são designadas por *scaffolds* e servem como suportes temporários para auxiliar e guiar a formação de novo tecido ósseo. As estruturas tridimensionais para poderem ser usadas na regeneração óssea têm que ser biocompatíveis, biodegradáveis, porosas e possuir propriedades mecânicas que promovam a osteoindução, osteocondução e neovascularização. Para atingir este fim, os investigadores têm usado vários materiais que incluem cerâmicas (hidroxiapatita), metais (titânio e cobalto), polímeros (colagénio e alginato) e compósitos dos mesmos em conjunção com métodos de prototipagem rápida, que permitem a criação de modelos produzidos através de programas informáticos ou através de dados recolhidos em exames de rotina em meio hospitalar.

Neste estudo foram produzidos *scaffolds* com uma geometria cilíndrica e, posteriormente, as suas propriedades químicas, mecânicas e biológicas foram caracterizadas. A forma cilíndrica foi escolhida com o intuito de mimetizar a geometria natural dos ossos ocos e permitir a troca de nutrientes e a sua neovascularização. Os *scaffolds* foram produzidos usando uma Fab@home 3D-Plotter. Este equipamento permite a extrusão de compósitos que permite a produção de matrizes com geometria complexa e poros interconectados. Os materiais usados neste estudo para a produção de *scaffolds* incluem o fosfato tricálcico e ácido algínico, que permitem reproduzir a matriz orgânica e inorgânica encontrada nos ossos. Por outro lado, procedeu-se ainda à produção de *scaffolds* contendo óxido de grafeno (GO) com o objetivo de melhorar as propriedades mecânicas e biológicas dos *scaffolds*. Os resultados obtidos neste estudo demonstraram que as amostras com óxido de grafeno possuem maior porosidade, sem que, no

entanto, a resistência mecânica dos *scaffolds* seja afetada. Adicionalmente verificou-se que a incorporação de GO não afeta o perfil citotóxico dos *scaffolds*. Os ensaios de biomineralização evidenciaram as capacidades osteoinductivas e osteoconductivas dos *scaffolds* produzidos, propriedades estas que são essenciais para a osteointegração destes *scaffolds* no tecido nativo. As propriedades mecânicas e biológicas apresentadas por estes *scaffolds* permitem postular a aplicação destes *scaffolds* na regeneração de tecido ósseo.

Futuramente, a performance in vivo destes *scaffolds* híbridos será avaliada em modelos animais de forma a averiguar o seu potencial osteogénico. Além disto, será otimizado o desenho dos *scaffolds* e para além do GO, serão também incluídos agentes com atividade antimicrobiana, na constituição dos *scaffolds*.

Abstract

The aging of the worldwide population has associated an increase in bone related traumas and diseases, that affect the well-being of human beings. Nowadays bone grafts, namely autografts, allografts and xenografts are used to treat these types of diseases. Yet these therapeutic approaches display several drawbacks such as limited tissue availability, chronic pain and possible immune rejection by the patient. To surpass these limitations, new therapeutic approaches are currently being developed to produce three-dimensional structures (scaffolds) that are capable of mimicking the mechanical and biological properties of native bone. Herein, cylindrical scaffolds were created using computer assisted design, with the aim of replicating the natural geometry of hollow bones and to allow the exchange of nutrients and neovascularization. A Fab@home 3D-Plotter was used for scaffold production. Tricalcium phosphate and alginic acid were selected for scaffold manufacture since they are able to reproduce the organic and inorganic matrix of bone. Furthermore, scaffolds were also functionalized with graphene oxide (GO) with the aim of improving the mechanical and biological properties of the scaffolds. The results obtained in this study demonstrated that GO bearing samples displayed increased porosity while maintaining their mechanical resistance. Additionally, the 60/40_GO scaffolds possessed an enhanced capability to adsorb calcium and phosphorous minerals, which give an important contribute for improving the osteoinductivity and osteoconductivity. In conclusion, the attained results revealed that GO functionalized 3D scaffolds have the desired properties that will allow their future application in bone tissue regeneration.

Keywords

Bone tissue engineering; Biocomposite 3D scaffolds; Rapid Prototyping; Graphene Oxide; 3D Printing;

Table of Contents

Chapter I

Chapter II

Chapter III

List of Figures

Acronyms

3DP	Three-Dimensional Printing
AA	Alginic Acid
ARRF	Activation-Resorption-Reversal-Formation
ARS	Alizarin Red Staining
ATR-FTIR	Attenuated Total Reflectance-Fourier Transformed Infrared Spectroscopy
BMU	Basic Multicellular Unit
BMP	Bone Morphogenic Protein
CAD	Computer Assisted Design
CSLM	Confocal Selective Laser Microscopy
DMEM-F12	Dulbeccos' Modified Eagles' Medium
ECM	Extracellular Matrix
EDS	Energy Dispersive Spectroscopy
EtOH	Ethanol
FBS	Fetal Bovine Serum
FDM	Fused Deposition Modelling
FGF	Fibroblast Growth Factor
GO	Graphene Oxide
HA	Hydroxyapatite
hOB	Human Osteoblasts
IGF-1	Insulin Growth Factor-1
IGF-2	Insulin Growth Factor-2
IL-6	Interleukin-6
MCP-1	Monocyte Chemoattractant Protein-1
M-CSF	Macrophage Colony-Stimulating Factor
MTS	3-(4,5-dimethylthiazol-2-yl)-5-(3-carboxymethoxyphenyl)-2-(4-sulfophenyl)-2H tetrazolium salt
NCP	Noncollagenous Proteins
PCL	Polycaprolactone
PTH	Parathyroid Hormone
RANK	Receptor of Nuclear κ-B
RANKL	Receptor of Nuclear κ-B Ligand
RGD	Arginine-Glycine-Aspartic Acid
RP	Rapid Prototyping
RT	Room Temperature
SBF	Simulated Body Fluid

SEM	Scanning Electron Microscopy
SLA	Stereolithography
SLS	Selective Laser Sintering
STL	Standard Tesselation Language
TCP	Tricalcium Phosphate
TE	Tissue Engineering
TGF-β	Transforming Growth Factor-β
TNF-α	Tumor Necrosis Factor-α
UV	Ultraviolet
WCA	Water Contact Angle
WGA	Wheat Germ Agglutinin
YM	Young Modulus

Chapter I

1. Introduction

1.1. Bone Tissue

Bone tissue is a specialized and dynamic connective tissue that acts as the basic unit of the human skeleton [1-3]. Bone tissue is responsible for supporting the human body and also other different biological functions, including locomotion, protection of vital organs (heart, lungs, spine and brain), mechanical support of the diaphragm and production of blood cells (hematopoiesis). Moreover, it also acts as a mineral reservoir, namely of calcium and phosphorous, and promotes muscle, ligament and tendon attachment [4, 5]. Bone tissue is under constant remodeling in order to allow this tissue to adapt to biomechanical forces and remove old and micro damaged bone.

Bone tissue is composed by cells (osteoblasts, osteocytes and osteoclasts), water and bone matrix. Such matrix is composed by organic (35%) and inorganic material (65%). The organic phase is composed of proteins of the extracellular matrix (ECM), collagen and proteoglycans. On the other hand, the inorganic phase contains calcium phosphate crystals, namely hydroxyapatite (HA) [6-8]. Bone cells are able to respond to external and internal biomechanical and biochemical stimulus that promote the cyclical demineralization/mineralization of bone tissue. In this process, osteoclasts remove old or damaged bone and osteoblasts are involved in the synthesis of new bone matrix [6].

1.2. Bone Anatomy and Morphology

The human skeleton is composed by several types of bones that can be distinguished according to their shape, morphology and bone matrix. According to their shape, bones can be classified as long, short, flat or irregular as shown in Figure 1.

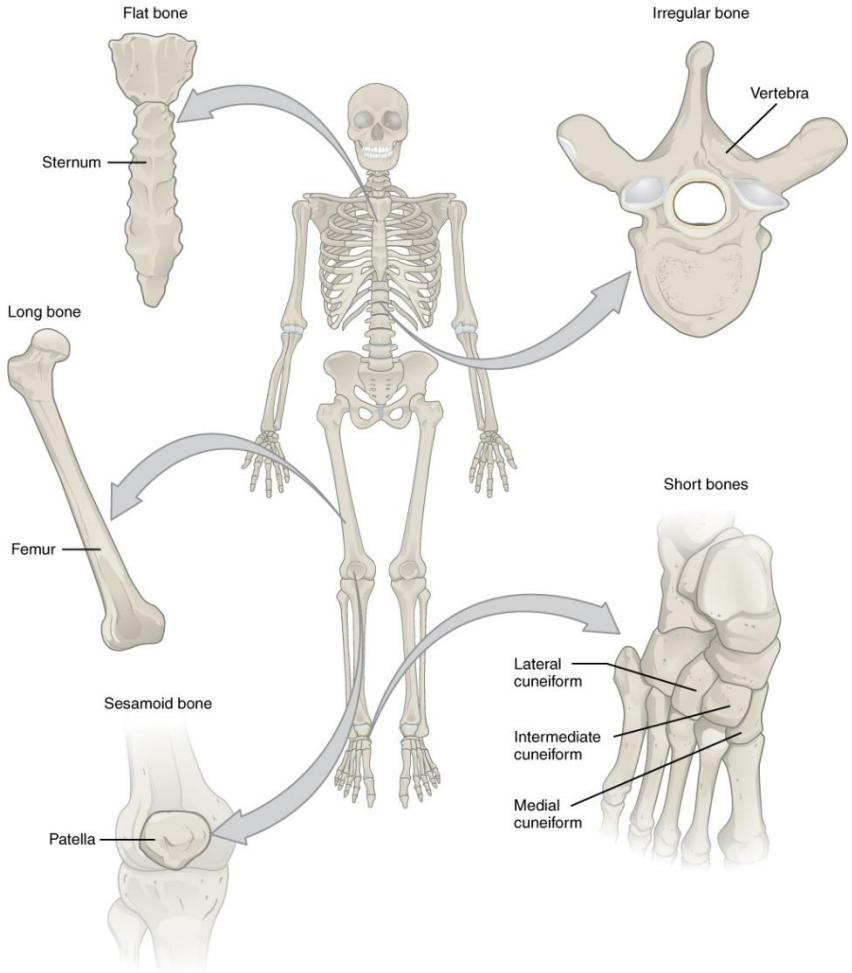

Figure 1. Classification of the bones according to their shape (adapted from [9]).

Long bones, such as clavicles, femurs and tibiae, have a cylindrical shape, great mechanical strength and durability. Short bones, like patellae, sesamoid, carpal and tarsal bones, have a roughly cube like or spherical geometry. For instance, flat bones present thin, curved or flat shapes and have a broad surface that is important for muscle attachment or organ protection (i.e. the bones of the shoulder girdle, ribs and breastbone). Finally, irregular bones have complex shapes that are neither long, short, or flat, such as the vertebrae and facial bones. These types of bones present many surface features for muscle or articulation attachment [10]. Morphologically, bone tissue is classified, depending on the density of the bone matrix, in trabecular or cancellous bone and cortical or compact bone [4, 5]. Cortical bone, represented in Figure 2, is almost compact, since it only presents a porosity of around 10% and accounts for 80% of the mass of a mature human skeleton [1, 6]. It has a high mechanical strength, since it is comprised of closely packed cortical osteons, called Haversian systems, that form a solid and consistent mass [7].

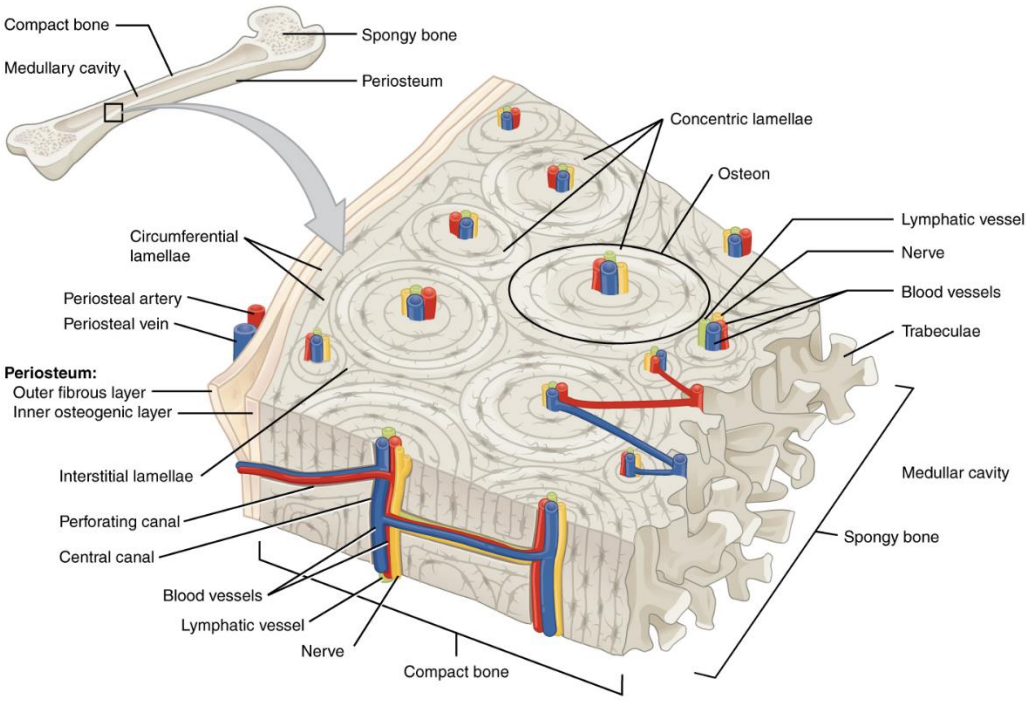

Figure 2. Cross-sectional view of compact bone showing the basic structural unit: the osteon (adapted from [9]).

The Harversian systems have a central canal, known as Haversian canal, that is surrounded by concentric rings of matrix and osteocytes that are responsible for its mechanical resilience [4, 7, 11].

The outer surface of cortical bone is covered by a bi-layered connective tissue membrane, shown in Figure 3, the periosteum. The outer, fibrous layer, is composed of irregular collagenous tissue, that contains blood vessels and nerves, while the inner layer is composed by a single layer of bone cells. These features facilitate the fixation of tendons and ligaments to the bone [12, 13].

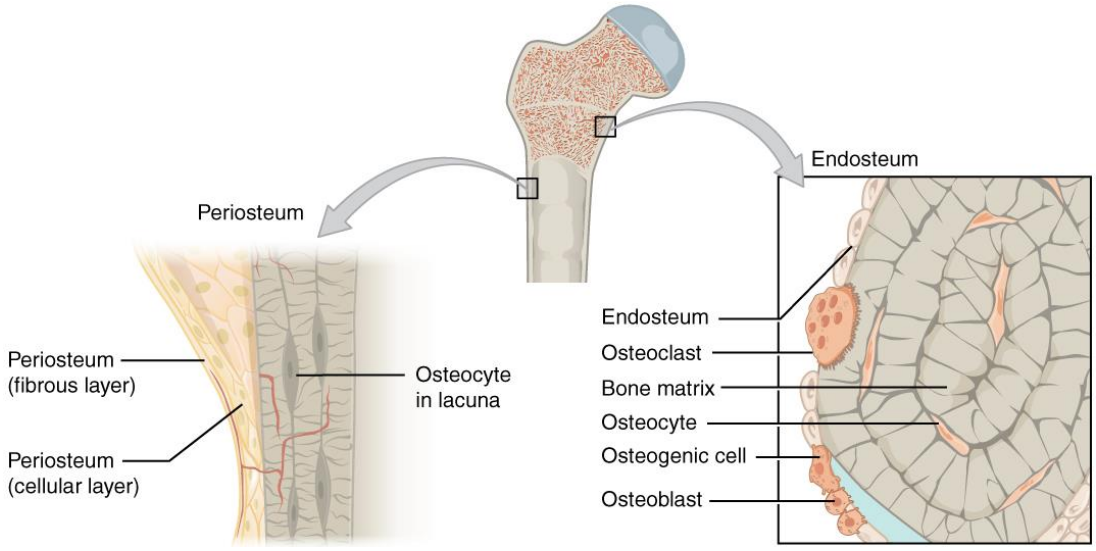

Figure 3. Illustration of bone Periosteum (the outer surface of the bone) and Endosteum (lines the medullary cavity) (adapted from [9]).

In contrast, the trabecular or cancellous bone is highly porous (50-90%) and has a compressive strength almost 20 times inferior to that displayed by cortical bone (2-20MPa for cancellous bone versus 100-200MPa for cortical bone [14]). It is strongly associated with metabolic activities, since its pores are interconnected and filled with bone marrow [1].

Cancellous bone, represented in Figure 4, has a sponge-like form, with a honeycomb of branching plates and rods of various sizes called trabeculae. In turn, the trabeculae are lined with another connective tissue membrane (endosteum), which is composed by a single layer of cells [4].

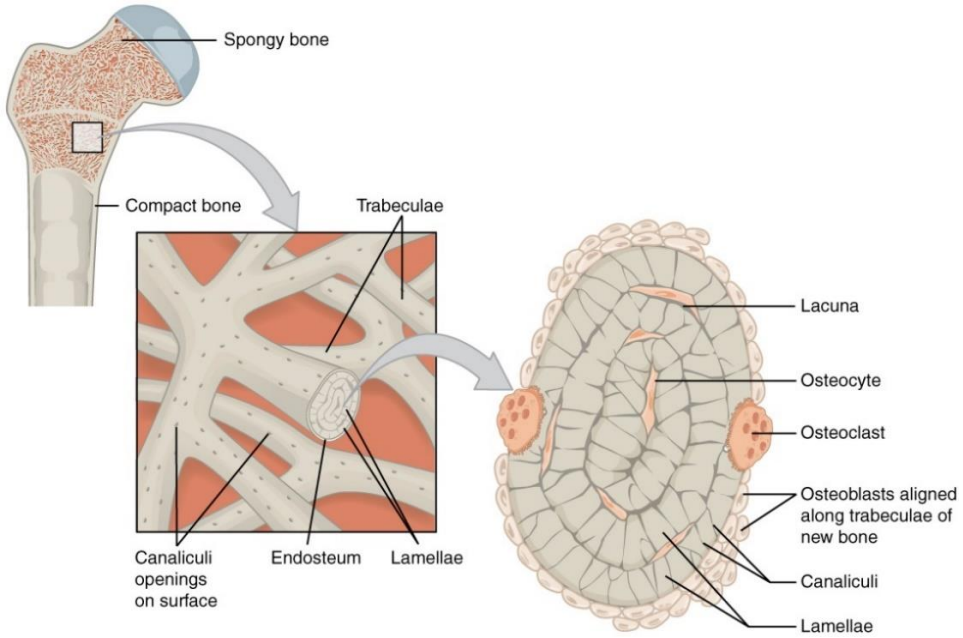

Figure 4. Illustration of the composition of spongy bone: trabeculae that contain the osteocytes. Red marrow fills the spaces in some bones (adapted from [9]).

Cortical bone, is found in the diaphysis of long bones. On the other hand, flat, short and irregular bone usually present a cancellous structure in their interior filled with marrow surrounded by two layers of cortical bone [10].

As represented in Figure 5, these two types of skeletal tissue can be found in long bones, the latter are divided in 3 different components, the diaphysis that composes the bulk of the bone, with a cortical periphery and cancellous interior; the epiphysis located at the ends of the bone, and the epiphyseal plate, made of cortical bone, and that is located between the diaphysis and the epiphysis, where the new bone is formed during bone growth [13, 15].

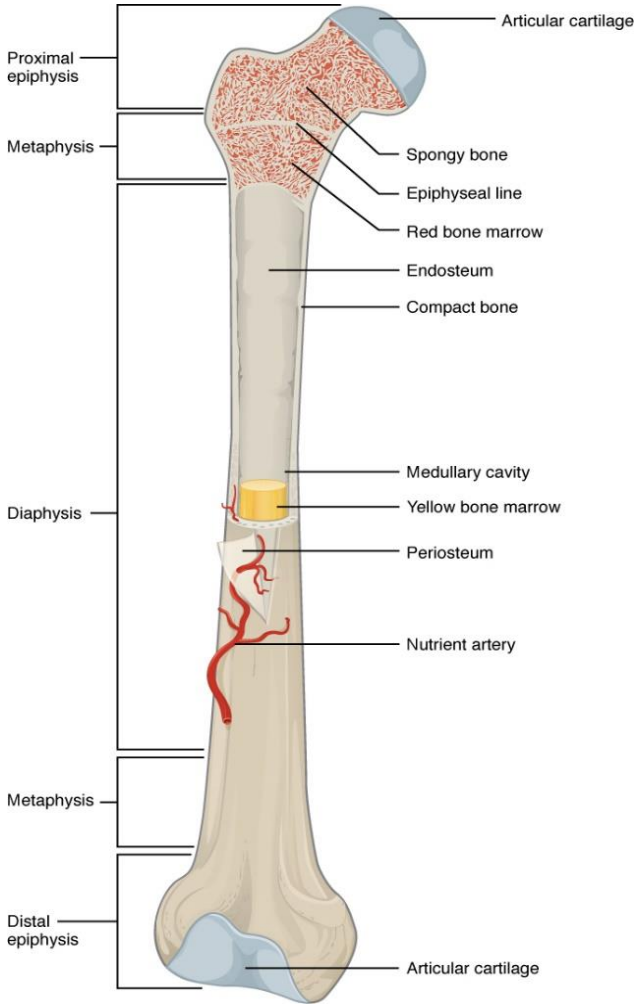

Figure 5. Representation of the anatomical characteristics of a long bone (adapted from [9]).

The diaphysis is an important structure present within long bones, which is filled with marrow. Blood cell formation occurs in the red marrow, while yellow marrow stores adipose tissue, acting as a localized energy reservoir in emergency situations, like bone fractures [10, 15, 16].

At the microscopical level, bone tissue can be further classified into woven or lamellar, according to the organization of the collagen fibers [7, 15, 17].

Woven bone presents randomly oriented fibers, which confer it weak mechanical resistance. It is characteristic of embryonic and fetal development, being found in the healthy adult skeleton

at ligament and tendon insertions and under pathologic conditions. Typically, it is remodeled to form lamellar bone [7, 17]. In contrast, the lamellar bone is a layered type of bone, composed of 3-7 μm lamellae, with collagen fibers lying parallel to each other, and with mineral crystals between them. This gives to the lamellar bone an increased strength [7, 15].

1.3. Bone Histology

1.3.1. Bone Matrix

Bone matrix is composed by an organic and mineral components with a ratio of 35/65%, which together contribute to the strength and flexibility of the human skeleton [5, 18, 19].
The organic phase comprises fibrillary proteins (mainly collagen type I), proteoglycans and a variety of noncollagenous proteins (NCP) that can be divided into structural proteins and promoters of biological processes [5, 7, 8, 20-23], whereas the mineral phase is mainly constituted by hydroxyapatite crystals. Although, tricalcium phosphate, calcium carbonate and fluoride derivatives can also be found in this matrix [18, 21]. It is estimated that bones contain 99% of the calcium, 85% of the phosphorus and 40-60% of the sodium and magnesium found in the human body [5, 21].
The balance between the organic and inorganic phases of the bone is crucial to confer to this tissue flexibility and resistance to compression (Figure 6). If the mineral component is diminished, the bone becomes more flexible, due to the increased collagen content. On the other hand, if the collagen percentage is diminished, the bone becomes very frail and brittle [15, 24].

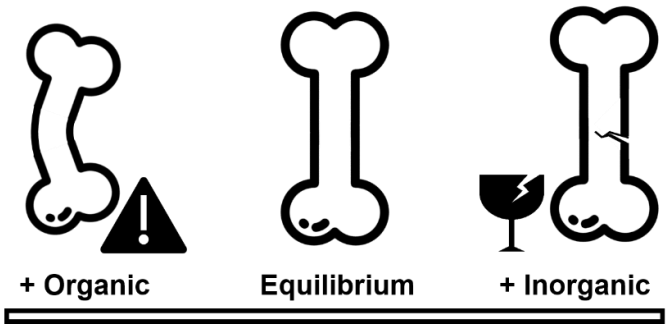

Figure 6. Illustration of bone phase composition effect on the mechanical behaviour of this tissue. Higher collagen content leads to excessive flexibility (left) while an excessive mineral content makes the bone brittle.

Besides that, bone matrix composition can also suffer variations with age, namely an increase in mineralization degree combined with a decreased bone collagen content [25, 26].

1.3.2. Bone cells

Besides osteogenic stem cells, bone is composed by three main cell types: osteoblasts, osteocytes and osteoclasts (represented in Figure 7), that are involved in the maintenance and remodeling process of the bone tissue.

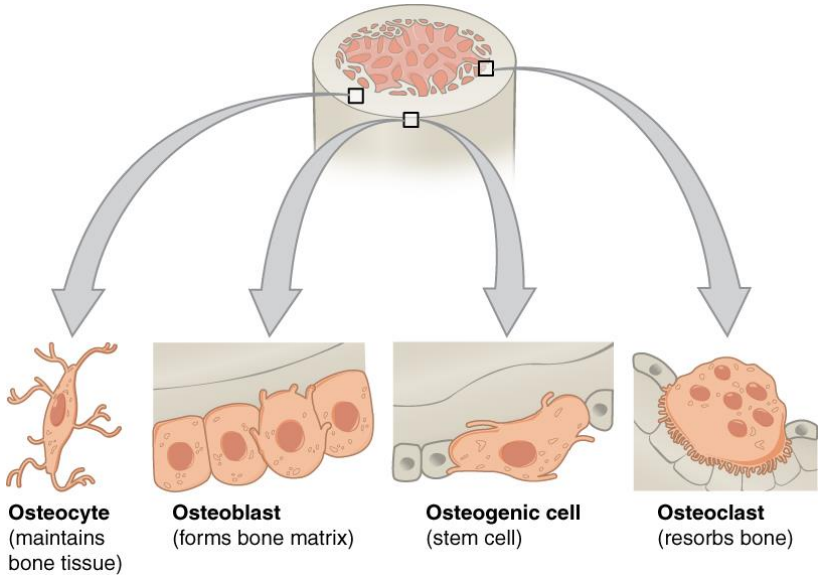

Figure 7. Representation of the types of cells found in bone (adapted from [9]).

1.3.2.1. Osteoblasts

Osteoblast are mononuclear and basophilic cells that display a large spherical nucleus, a highly developed rough endoplasmic reticulum and Golgi apparatus [7]. These cells are derived from mesenchymal stem cells and are present at bone surfaces [18, 27]. Structurally they have a cube-like shape or a slightly elongated appearance [7]. They are involved in the synthesis and organization of the bone ECM, that subsequently becomes mineralized [6, 7].

Moreover, osteoblasts contain vesicles loaded with phosphate, calcium ions and enzymes (ie. alkaline phosphatase), that are released by exocytose and that are involved in hydroxyapatite crystal formation, thus promoting bone mineralization [15]. These cuboid shaped cells can produce 0.5-1.5µm of osteoid per day and display an average lifespan of 8 weeks in humans [7].

It is noteworthy to stress that osteoblasts after that become differentiated may have three

When osteoblasts become surrounded by fates: revert back to bone lining phenotype (quiescence phase); differentiate into osteocytes or underdo apoptosis [20, 21].

1.3.2.2. Osteocytes

bone matrix they differentiate into osteocytes [28, 29]. The primary function of osteocytes is to maintain the bone structure since they act as mechanosensors capable of transducing musculoskeletal stress signals, guiding bone remodeling [28, 29]. Currently, it is proposed that these cells modulate the spatial and temporal formation and resorption of bone tissue, through

the high number of dendritic processes that interconnect the osteocytes and bone lining cells [7, 15, 28]. They form filopodia located in spaces or channels in the bone matrix called canaliculi. The arrangement of the canaliculi allows the passage of nutrients, metabolites and oxygen between the blood vessels and distant osteocytes [7, 21, 30]. Also, Nitric oxide, Wnt and cadherin-mediated signaling have been suggested as transducing mechanisms, since they are activated after a mechanical stimulus [31, 32]. However, the precise mechanisms of stimulus and response remain unclear. Osteocytes are also responsible for osteocytic osteolysis, i.e., breaking down the bone matrix to release calcium that is required for other metabolic pathways [20].

1.3.2.3. Osteoclasts

Osteoclasts are cells, that derive from hematopoietic stem cells, and that are involved in the resorption of fully mineralized bone, leading to the mobilization of Ca^{2+} and PO_4^- ions from the bone matrix [5, 7, 20]. They are highly specialized and multi-nucleated giant cells.
During their motile state, they migrate from the bone marrow to their resorptive site where they will initiate bone resorption. In this state, they present a flat and non-polarized morphology, with membrane protrusions such as lamellipodia and actin rich podosome complexes. On the other hand, in their resorptive state they assume a polarized shape. In this phase the cells display a dome shape (that results from cytoskeletal reorganization) and new membrane domains (such as the sealing zone) are formed [5, 30, 33].
Osteoclast cells present numerous mitochondria, a well-developed Golgi apparatus around the nuclei, endoplasmic reticulum, vacuoles and lysosomes. This cellular organization results from their great involvement in protein synthesis, in particular lysosomal enzymes, as well as their excretion into the resorptive bay along with acidic compounds that take part in bone resorption process [34]. Through this complex cellular machinery, osteoclasts are capable of resorbing up to 200 000μm^3/day of bone matrix and they have an average lifespan of 15-20 days [7].

1.3.3. Bone Remodeling Process

Bone is a dynamic and metabolic active tissue that is constantly being remodeled. The remodeling process consists in the resorption of old bone and on the formation of new bone in order to prevent the accumulation of micro damages, like nanocracks and thus assure the homeostasis of the skeletal tissue [4, 5, 35].
Yet, to accomplish that a careful balance between bone resorption and formation must be kept. Within this process, osteoblasts and osteoclasts operate in an orchestrated manner, gathering in a temporary assembly a basic multicellular unit (BMU) on the bones' surface [6, 28, 36, 37]. In these BMUs cell activity is sequential: first, osteoclasts in the leading edge of the BMU resorb damaged or old bone; followed by osteoblasts that at the end of the BMU secrete collagen fibers and mineralize the matrix to form new bone (see Figure 8 for further details). This unit

is regulated by mechanical forces, bone cell turnover, hormones (PTH (pituitary hormone), growth hormones, etc), cytokines and local factors [6].

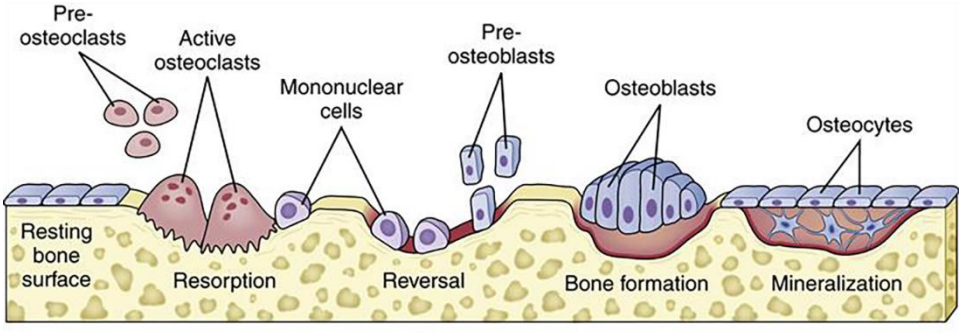

Figure 8. Schematic representation of the different phases and acting cells in the bone remodeling process. Initially a biochemical or biomechanical signal promote pre-osteoclast migration to its resorptive area. In the Resorption phase, mature osteoclasts in the Howship lacunae actively resorb the damaged or old bone. In the Reversal phase pre-osteoblasts are recruited into the area and differentiate into mature osteoblasts. During the Formation phase, osteoblasts actively secrete organic matrix (collagen type I) and initiate its mineralization. Finally in the Formation phase the organic matrix is fully mineralized, osteoblasts either undergo apoptosis or differentiate into osteocytes or bone lining cells (adapted from [38]).

The bone remodeling process comprises four main phases (activation, resorption, reversal and formation stages (ARRF sequence), as shown in Figure 8) and it lasts about 3-6 months before its fully complete in humans [36]. Moreover, bone remodeling is not only required to replace dead or damaged tissue, but also confers bone the capacity to adapt to loading variations or respond to nutritional and metabolic changes.

Activation phase

The first stage of bone remodeling involves the detection of an initiation signal, like mechanical strain, damage or biomolecules released into the bone microenvironment [31, 36]. In response to these stimulus, osteoblasts start recruiting osteoclast precursors to the remodeling site, through the release of a chemoattractant, MCP-1 (monocyte chemoattractant protein) [35]. In case of structural damage, insulin growth factor-I (IGF-I), tumor necrosis factor-α (TNF-α), parathyroid hormone (PTH) and interleukin-6 (IL-6) promote the activation of bone lining cells present on bone surface, leading to an increased expression of the receptor activator of nuclear factor κ-B ligand (RANKL) at the surface of these cells. On the other hand, in response to the osteoclastogenic stimulus, pre-osteoblasts secrete macrophage colony-stimulating factor (M-CSF), that induces the expression of Receptor Activator of Nuclear κ-B (RANK) by osteoblasts. The RANKL/RANK interaction triggers pre-osteoclasts fusion and differentiation toward mature osteoclasts [36, 37]. In addition, bone damage or immobilization can result in osteocyte apoptosis, leading to an increased osteoclastogenesis. [30, 31].

Hormones may also trigger osteoclast activation and differentiation. PTH acts as an endocrine remodeling signal involved in the maintenance of calcium homeostasis. This hormone is secreted by the parathyroid glands in response to low calcium levels in the blood serum, and can lead both to bone formation, when secreted intermittently, or to bone resorption when secreted continuously [6, 35]. In bone tissue, PTH activates the PTH receptor (a G-protein-coupled receptor found on the surface of osteoblasts) [30], that activates protein kinase A, protein kinase C and intracellular calcium signaling pathways. This osteoblast activation causes a wave of transcriptional responses that modulate the secretion of molecules responsible for the recruitment, differentiation, and activation of osteoclasts, which are one of the main players in bone resorption [18, 35].

Resorption phase

The resorption phase, which lasts on average 30-40 days, consists in the attachment of differentiated osteoclasts to depressions or resorptive bays (known as Howship lacunae) present in the bone matrix [35, 36]. Cell anchorage is performed via $\alpha_v\beta_3$ integrin molecules, upon adhesion, osteoclasts suffer cytoskeletal reorganization creating an isolated microenvironment underneath the cell, known as the sealed zone [18]. Subsequently, osteoclasts promote the bone demineralization process, in two steps [36]:

i) acidification of the bone matrix though proton pumps, that leads to a higher concentration of hydrogen ions in the sealed zone [35, 36, 39]
ii) release of lysosomal (e.g. cathepins K) and non-lysosomal (e.g. collagenase) enzymes that are involved in the degradation of the organic component of the bone [18, 35]. This exposes arginine-glycine-aspartic acid (RGD) sequences that enhance osteoclast attachment and consequently increase bone resorption [35]. To avoid excessive bone resorption, osteoclasts suffer apoptosis after this stage.

Reversal phase

Reversal phase marks the transition from osteoclast to osteoblast activity, with osteoblast precursors being recruited and differentiated into their mature state [39, 40]. This phase lasts approximately 9 days, and during this period, bone lining cells (mononuclear cells of osteoblastic origin) prepare the bone surface for the subsequent bone deposition performed by osteoblasts [30, 35, 36]. This stage is also characterized by the presence of activation of factors (IGF-2 and TGF-ß) that stimulate osteoblast precursors to proliferate [7, 35, 36].

Formation phase

The formation phase is characterized by the release of a variety of growth factors stored in the bone matrix, such as bone morphogenic protein (BMP), fibroblast growth factor (FGF) and TGF-ß that are responsible for the recruitment of osteoblasts into the absorbed area [33, 41]. At this stage, differentiated osteoblasts synthetize new organic matrix (collagen type I) and

release vesicles that contain calcium, phosphate and enzymes that destroy the mineralization inhibitors, such as pyrophosphate or proteoglycans [7, 30, 35, 36].

The remodeling cycle is concluded when all reabsorbed bone is replaced. At the end of the cycle, osteoblasts either suffer apoptosis, revert back to bone lining phenotype, or differentiate into osteocytes that remain within the matrix [30, 41]. Even though the bone remodeling process is one of the most reliable biological process in the body, there are circumstances where it fails. Indeed, bone disorders are almost always related to the deregulation of this cycle, influencing either bone formation or resorption [33, 42]. Such can compromise the architecture, structure and mechanical strength of bone tissue, leading to clinical symptoms such as pain, deformity, fractures and abnormalities of calcium and phosphate metabolism.

1.4. Bone Disorders

Bone defects can be caused by trauma, tumors, infection or bone diseases. Bone diseases comprise abnormal bone growth, that can lead to gigantism or dwarfism; abnormal collagen contents that can lead to osteogenesis imperfecta; Mineral and vitamin deficiencies cause rickets; bacterial infections that can provoke bone destruction, as is the case of osteomyelitis [30, 43]; Osteomalacia and osteoporosis are also responsible for bone damage through decalcification [15]. Figure 9 represents three of the most common disorders associated with bone tissue.

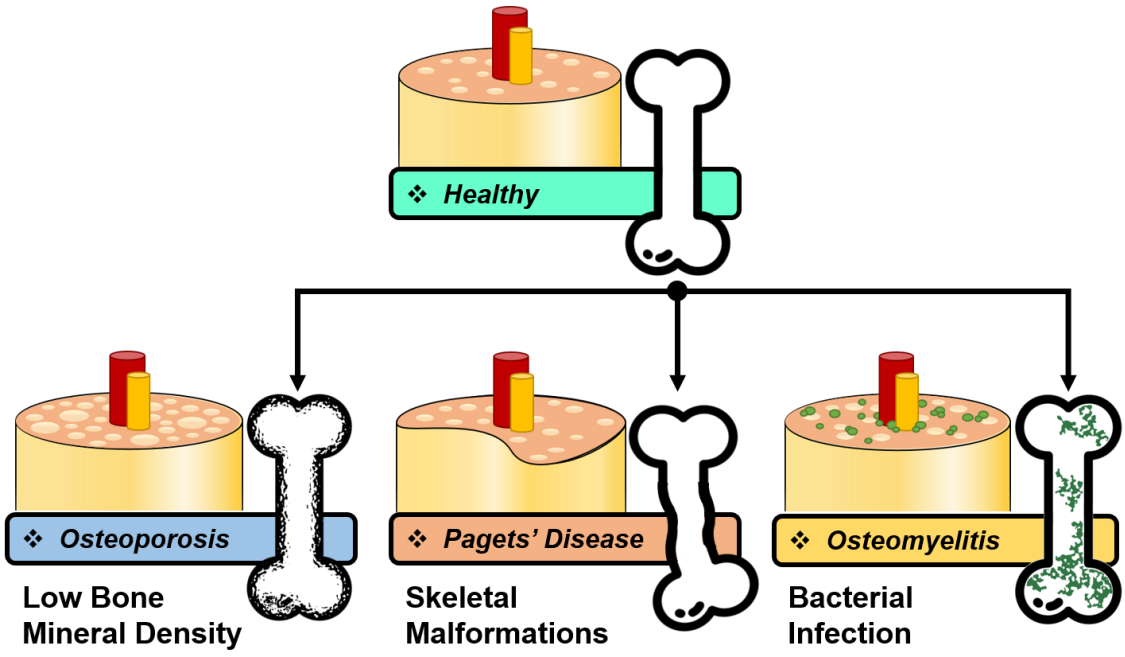

Figure 9. Representation of the most common bone diseases and their effects on bone.

1.4.1. Osteoporosis

Osteoporosis is the most common disease affecting bone [44]. A study performed in 2010 estimates that 27.5 million people were affected by the disease only in the European Union [45]. Osteoporosis is characterized by low bone mass and structural deterioration, causing an increased bone fragility and vulnerability to fractures. This disorder is more common in older populations, especially in women, due to menopausal estrogen deficiencies that increase the bone resorption [33]. This disease usually results from an imbalance between bone resorption and bone formation [21, 30, 42, 46]. It is believed that sex steroid hormones, either directly or indirectly, regulate the production of cytokines (e.g. M-CSF) that promote the production of osteoclasts [42, 47].

Nevertheless, excluding the hormonal effects of menopause, this disease has the same rate of progress in both genders [44].

The most common osteoporotic fractures occur in the hip, vertebral column, and forearm. These fractures may result in morbidity or in severe cases can lead to patient death [33]. Unhealthy diet, sedentary lifestyle, nulliparity, aging, smoking, and low body weight are also risk factors that may trigger the development of osteoporosis [21].

1.4.2. Pagets' Disease

Pagets' is the second most common bone disease [30]. It is characterized by focal areas of excessive bone resorption, alternated with areas of increased bone formation, leading to the formation of abnormal bone, pain, pathologic fractures, deafness and nerve compression syndromes [30, 33, 46, 48, 49].

Although the causes are not entirely known, it is believed that this disease can be provoked by a viral infection during childhood, and several genetic mutations have also been identified on patients with this disease [39, 44, 49]. Nevertheless, sedentary lifestyle and deficient nutrition are also reported as factors that may be involved in the Pagets' disease arising.

1.4.3. Osteomyelitis

Osteomyelitis is defined as an inflammation of bone tissue accompanied by its destruction, due to microbial infection [43, 46, 50]. Moreover, it can also be caused by fractures that occur due to trauma or other diseases [46]. Upon fracture, microorganisms (like *Staphylococcus aureus*) produce a range of extracellular components and cell-associated factors, that facilitate its colonization capacity and virulence [43].

1.5. Bone Grafts

As previously described, there are certain critically sized osseous defects that the organism is unable to heal without medical assistance [51]. In such cases, bone grafts have been used for bone tissue reconstruction. The capacity of bone grafts to regenerate tissue is measured by their osteogenic, osteoconductive and osteoinductive potential [52]. The bone grafts are divided into three main categories: autografts, allografts and xenografts as represented in Figure 10 [52]. Nowadays, autografts are the most used for bone tissue regeneration. However, their use is limited due to the low availability of graft tissue and considerable donor site morbidity, which is proportional to the amount of harvested bone [51, 53, 54]. Furthermore, the harvesting procedure induces bleeding, hematoma, infection and in some cases chronic pain to the patients [52, 55, 56]. In addition, there is no guaranty that the cellular components survive the transplantation [56], and questions have been raised about the osteoinductivity of these grafts, since the uncertainty about the grafts' growth factor content can lead to insufficient tissue regeneration [57]. To overcome the lack of autografts, allografts have also been used for bone tissue replacement. However, since the grafts are from different donors (of the same species), there is always a risk of disease transmission and of triggering of an immune response from the host [51, 52, 55, 56]. Unfortunately the processing techniques used to decrease the associated risks also reduce the mechanical resistance of the grafts, and usually remove the cellular component from the bone tissue [56].

Xenografts are obtained from different species, which can lead to the rejection of the graft by the host. To overcome this drawback the biological components are removed in order to increase the safety of grafts [55].

Due to all aforementioned limitations, bone graft substitutes have been the focus of intense research in the area of Bone Tissue Engineering [58]. This area intends to develop three-dimensional (3D) structures capable of mimicking the bone structure and microenvironment [52].

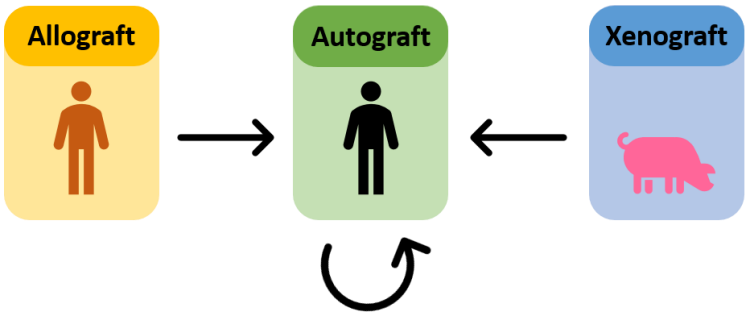

Figure 10. Illustration of different therapeutic approaches.

1.6. Tissue Engineering

Tissue Engineering (TE) is an interdisciplinary field of research that applies the principles of engineering and life sciences, to develop new therapeutic approaches that allow the restoration, maintenance or improvement of a particular tissue function [2]. In particular, bone tissue engineering aims to produce grafts with the capacity to induce the restoration of bone structure and functions (Figure 11) [14, 20, 58-61].

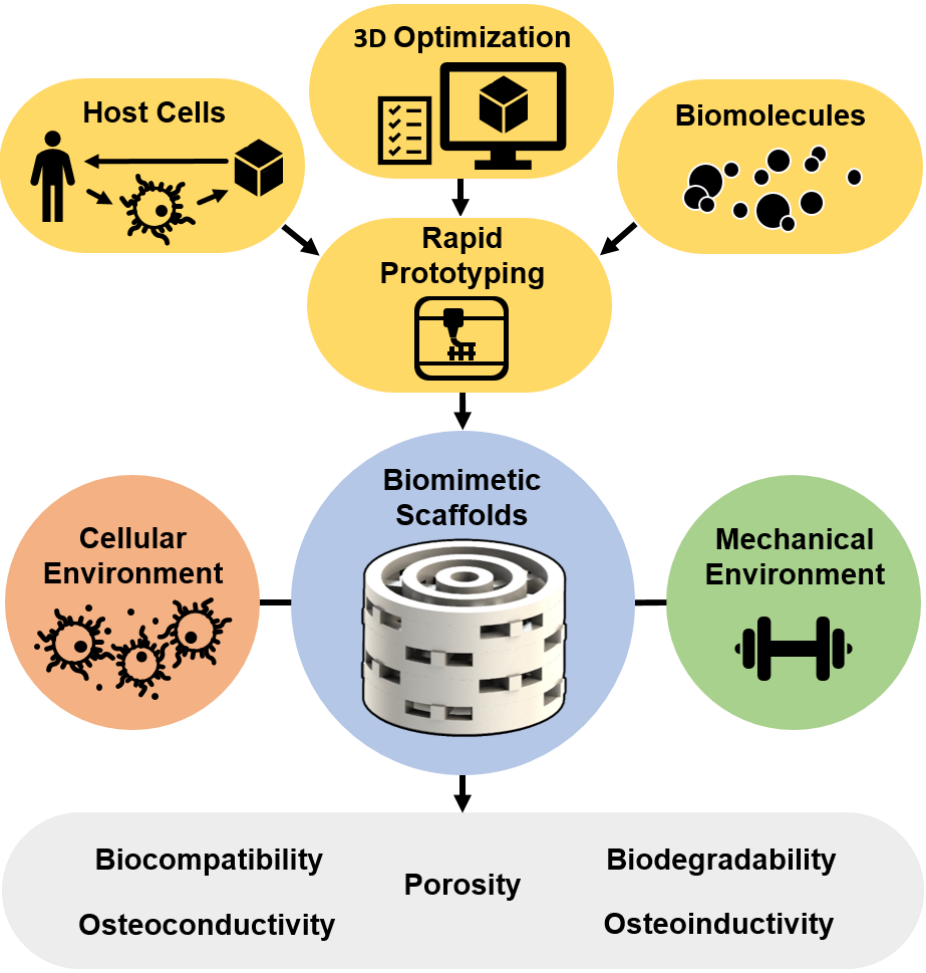

Figure 11. Experimental approach used to develop biomimetic 3D scaffolds.

Nonetheless, scaffold production is limited by the current manufacturing techniques, and also by the random distribution of cells, matrix and bioactive molecules within the scaffolds' structure. As such, mimicking the functional and biological complexity of bone tissue is seen as the current challenge to achieve full tissue regeneration [62].

1.6.1. 3D Scaffolds

Scaffolds are porous 3D matrices that act as temporary templates, that allow cell adhesion and proliferation, as well as provide mechanical support until new bone tissue is formed at the defect site.
Scaffolds have been produced using a variety of techniques, such has selective laser sintering (SLS) [63], 3D printing (3DP) [64], stereolithography (SLA) [65] and fused deposition modelling (FDM) [66], using different biomaterials that present certain key properties (biocompatibility, biodegradability, surface properties, porosity and mechanical properties) that are fundamental for scaffolds to promote osteoinductivity, osteoconductivity of bone-producing cells and neovascularization [14, 67-70].

- **Biocompatibility**

Biocompatibility is considered one of the most important properties that any type of implant or biomedical device must display [17]. Biocompatibility represents the ability of a material to support normal cellular activity including adhesion, proliferation and differentiation without eliciting any local or systemic response from the immune system [14, 58, 67]. Generally, scaffolds should be produced from materials that do not trigger any immunogenic reactions. Furthermore, the degradation products of the scaffolds must also be biocompatible and easily removed from the body [67, 71].

- **Biodegradability**

A scaffold aimed for bone regeneration may be designed to serve as a temporary matrix, and eventually, be replaced by bone tissue. In addition, the degradation products of the scaffolds must not elicit any adverse effect on the host [14]. The scaffolds' degradation rates ideally should accompany the rate of regeneration of new bone [58, 60, 71]. As a result, a scaffold must be completely degraded when the injury site is totally regenerated. Moreover, the rate of scaffolds degradation depends on the extent and site of the injury, on the biomaterial used for scaffold production as well as on the production technique employed.

- **Surface properties, osteoconductivity and osteoinductivity**

The scaffolds' properties comprise their surfaces' hydrophobic/hydrophilic character, charge, roughness, softness and chemical composition [67, 71]. Such features are determinant for controlling cellular adhesion and proliferation [2]. Osteoconduction is a process in which bone cells produce a fibrin clot around the implant, that acts as a structural support for maintaining

the implant at the lesion site and also provide structural integrity to the injury location. Moreover, the clot can serve as a bridge for cells to migrate from the surrounding bone tissue to the scaffolds' surface [2, 14, 51]. On the other hand, osteoinduction is a process by which the osteoprogenitor cells are stimulated to undergo osteogenic differentiation [67]. Hence, the use of osteoconductive and osteoinductive materials in bone tissue regeneration are required for bone structure and function to be reestablished [2]. The rough and positively charged surfaces promote the osteoconduction, creating a matrix that enhances cell adhesion and proliferation [14, 60, 67, 72]. In addition, the scaffolds may also release osteoinductive signals through the action of growth factors or bioactive molecules that induce differentiation of bone cells [2, 51, 67].

- **Mechanical Properties**

In order to provide adequate mechanical support until the new bone is fully matured, a bone scaffold must have mechanical properties that fulfill all the requirements of the host bone [14, 58, 60, 67, 68]. Young's modulus presented by cortical bone is comprised between 15-20GPa, while for cancellous bone it is between 0.1-2GPa [14]. In turn, the compressive strength is comprehended between 100-200MPa for cortical bone, and 2-20MPa for cancellous bone [14]. Since these properties depend on bone type and location, scaffolds must be tailored for a specific application, taking into account the loads that they will have to bear once implanted.

Additionally, finding a harmonious balance between scaffolds' mechanical properties and their degradation kinetics is essential, since this grants integrity to the fracture site while scaffold degrades and new bone is formed [60, 67].

- **Porosity**

The porosity is defined as the percentage of void spaces available inside of the scaffolds. The scaffolds must possess pores with inter-connectivity among them, to ensure the nutrients and gaseous exchanges within the scaffold, processes that are crucial for maintaining cell viability and promoting bone regeneration [14, 17, 67]. Taking this into consideration, an ideal 3D scaffold should have a suitable interconnected porosity (higher than 90% to replicate trabecular bone) to allow cell penetration, differentiation, and consequently improve new bone tissue formation [54]. Additionally to facilitate bone ingrowth, scaffolds must possess pores with a minimum diameter of 100μm, with an ideal range comprehended between 200-300μm [14]. The pores size and distribution must be tailored so that biological functions and mechanical stability of the scaffolds are preserved. It is known that scaffolds with a high porosity tend to present lower mechanical properties and higher degradation rates [58, 67, 71]. Thus, it is important to

develop a 3D scaffold that provides the best compromise between porosity, mechanical performance and degradation rates.

1.6.2. Biomaterials for scaffold fabrication

Scaffolds composition will be decisive for their performance, since the materials used for their production will ultimately be responsible for the properties displayed by the scaffolds. Several materials (ceramics, metals, polymers and composites) have been employed so far in the production of 3D scaffolds that meet the requirements mentioned in the previous section [53, 60, 73].

1.6.2.1. Ceramics

Ceramic based scaffolds usually present high mechanical stiffness, low elasticity and hard surface [2]. 3D scaffolds are usually produced using calcium rich substances like hydroxyapatite (HA) and tricalcium phosphate (TCP, shown in Figure 12) [2, 19, 53, 73].

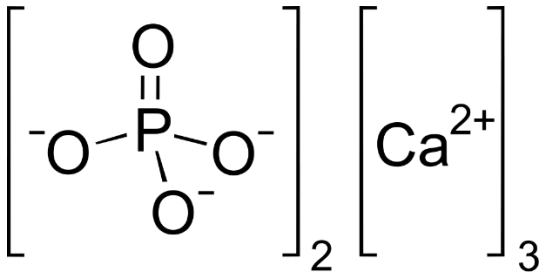

Figure 12. Chemical structure of tricalcium phosphate.

These materials represent valuable options for bone tissue engineering applications, since they display an excellent biocompatibility. Furthermore, they also have a chemical and structural resemblance to the mineral phase of the native bone tissue [53, 67, 74]. Additionally, these materials are also able to promote interactions with osteogenic cells, thus enhance osteoblast differentiation, proliferation which in turn aids in the bone healing process [19, 75]. These bioactive ceramic materials have also shown to induce surface mineralization which is fundamental for scaffold bio-integration, and consequently enhance bone regeneration [19, 67]. However, these materials present distinctive degradation rates. While TCP presents an almost ideal biodegradation *in vivo*, HA displays a very low degradation rate [17, 70, 76]. In addition, the ability of TCP to bind directly to tissue, and regenerate bone without intermediate tissue, as well as display a proper bio-resorption rate, have made it one of the most used ceramics in tissue engineering [14, 17, 52, 76, 77]. Nonetheless, these materials have some

limitations, like brittleness and shape related issues that decrease their applications in the clinic [73].

1.6.2.2. Metals

Metals are characterized by presenting a great compressive strength and fatigue resistance [75]. Titanium is mostly used for scaffold production, due to its mechanical properties. However, they are not biodegradable and require coatings and surface treatments to allow the immobilization of biologically active molecules on their surface [14, 78].

1.6.2.3. Polymers

Polymers are macromolecules formed by repetition of one or several subunits, that have excellent biological properties such as biodegradability, biocompatibility, flexibility and bioactivity. Such features make them very suitable materials for bone tissue engineering applications [20, 58, 67, 73]. The polymers can be categorized as natural and synthetic, according to their source [79].

- **Natural Polymers**

Natural polymers are obtained directly from natural sources, such as animals and plants. Up to now there are several natural polymers that have been used in bone tissue engineering like: Alginic Acid ((AA) obtained from brown seaweeds); Cellulose (obtained from plants); Chitosan (obtained from crustaceans); Silk (obtained from plant sources); Collagen, Gelatin and Hyaluronic acid (obtained from animal tissues upon proper treatment) [20, 75, 80].

These materials usually present a high cytocompatibility and low risk of immunogenic response [75, 79, 81]. On the other hand, the limitations of naturally derived polymers include weak mechanical behavior, fast degradation rates and in some cases have associated hard processing and purification steps [74, 75, 81].

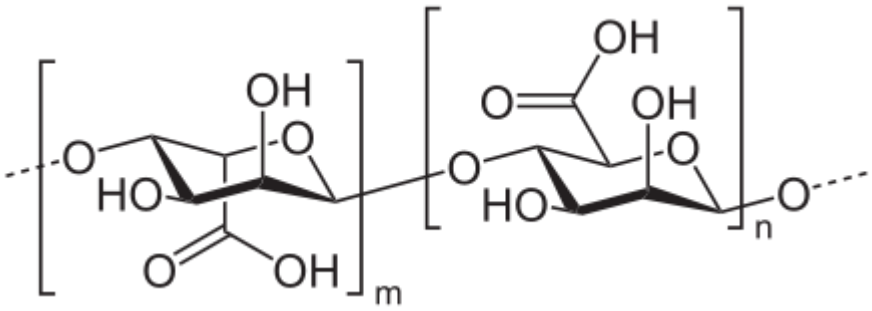

Figure 13. Chemical structure of alginic acid.

AA is an example of a natural polymer (depicted in Figure 13) and it is composed by ß-d-mannuronate (M) and α-l-guluronate (G) [82]. The physical properties displayed by this material are strongly influenced by the chain length as well as the ratio of G residues [82, 83]. AA with a high content of G residues becomes a stiff and stable material, whereas the polymer with a low content of G residues becomes a more elastic and less mechanically stable material [83, 84]. In addition, this polymer can form stable hydrogels cross-linked with divalent cations. This crosslinking happens between two G blocks of adjacent polymer chains, through the interaction with the carboxylic groups. Hence, the stiffness of the produced gel is directly proportional to the M/G ratio of the polymer and to the amount of free divalent cations available in solution [82-84]. Still the dissolution of ionically cross-linked alginates cannot be perfectly controlled, and it presents slow degradation profiles *in vivo*.

- **Synthetic Polymers**

Synthetic polymers are chemically synthetized and are widely used in the bone tissue engineering field, due to their high reproducibility and versality [14, 58, 67, 81]. Generally, they have enhanced mechanical properties although they are less biocompatible, when compared to natural polymers. PCL as a synthetic material, is an aliphatic, linear polyester, which is synthesized through ring-opening polymerization of ε-caprolactone [14, 58]. Despite its biocompatibility and ability to be resorbed by the human body, it has a hydrophobic nature that severely limits cellular adhesion and interaction with other biological components [14].

1.6.2.4. Graphene Oxide

One of graphenes' derivatives, Graphene Oxide (GO) has received special focus due to its high surface area-to-volume ratio, enhanced mechanical properties, osteogenic potential and biocompatibility [85, 86]. This 2D nanomaterial consists of a single layer of sp^2-hybridized carbon atoms in a hexagonal lattice conformation, displaying carboxyl, hydroxyl and epoxy

groups on its edges and basal planes, as shown in Figure 14 [87-89]. These oxygen functional groups confer GO a good dispersibility and hydrophilicity.

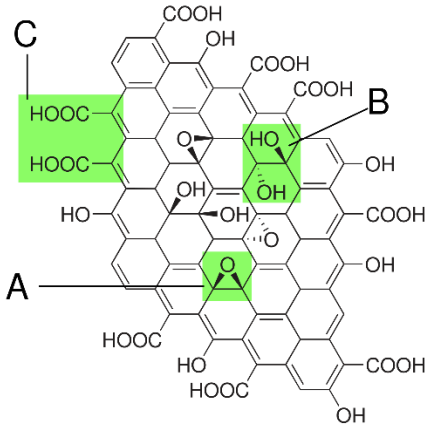

Figure 14. Molecular representation of a GO flake. Highlighted in green are its groups: epoxy (A); hydroxyl (B) and carboxyl (C).

In recent years it has been demonstrated that by performing GO incorporation in composite materials their mechanical strength could be increased [88, 90]. This property confers GO a good potential for being applied in bone tissue engineering.
Moreover, GOs' charged chemical groups and surface area have been correlated with its potential to promote cell adhesion, proliferation and differentiation towards the osteogenic lineage, without the need for osteogenic factors [91]. Additionally, GO has also been linked to enhanced osteoinductivity and osteoconductivity by promoting surface adsorption of minerals (calcium and phosphate) that improve cellular attachment and osteointegration of organic/inorganic composite scaffolds aimed for bone tissue regeneration [92-94].

Furthermore, several studies have shown that GO is biocompatible [85, 86] and that it can suffer extracellular biodegradation, making it suitable for bone tissue engineering applications [95].

1.6.2.5. Composites

Composite materials have in their constitution two or more distinct materials, for example ceramics and polymers [14, 19]. These combinations aim to mimic the structure of the native bone (organic and inorganic matrices) and try to overcome the drawbacks of the brittleness of ceramic scaffolds by adding a polymeric compound, that is inherently more flexible [96]. The ceramic/polymer combinations allow the production of structures with an excellent balance between strength, toughness and flexibility, making them more suitable for bone tissue engineering applications [73, 96].

1.6.3. Techniques used in scaffold fabrication

In order to produce scaffolds aimed for bone regenerating applications various techniques can be used [58, 97-99]. Until now, the most used included particulate leaching [100, 101], gas foaming [102, 103], solvent casting [104-106], vapor deposition [107, 108] and freeze drying [109, 110]. These methods allow the reliable production of macroscopic 3D structures. However, they present some disadvantages, such as the use of toxic solvents, the inability to create large structures with suitable mechanical properties or lack of precise microstructure and porosity control [111]. The advances in computer technology allowed the development of rapid prototyping (RP) techniques that can be used to produce 3D scaffolds for tissue engineering applications. Several new methods have been developed for the accurate fabrication of complex 3D structures [97, 98, 111-113], such has selective laser sintering (SLS) [63], 3D printing (3DP) [64], stereolithography (SLA) [65] and fused deposition modelling (FDM) [66]. These techniques enable the manufacturing of highly reproducible 3D scaffolds, with increased complexity and interconnected porosity [14, 97, 99, 112, 114]. Moreover, the model used for scaffold production can be based on medical data, and thus be tailored specifically for a particular damaged tissue with high anatomic accuracy [114-116].
One of the most used RP techniques in the area of tissue engineering is 3D plotting [1, 117]. In 3D plotting a blend is dispensed through a syringe onto a platform. The deposition can be achieved by pneumatic action, screw-driven, or piston action, with the latter providing the best flow control. The robotic deposition has resolutions of the order of 200μm, with high fabrication speeds, and is one of the most promising technologies in the field [62].
In this work, a Fab@home 3D plotter was used for scaffold production which has been previously used for tissue engineering applications [118-120].

1.6.3.1. Scaffold fabrication with a Fab@home 3D Plotter

The Fab@home model has advantages over other equipment, allowing the employment of different samples, like composites and viscous solutions, as hydrogels. However, the printing accuracy and resolution of the extruded materials depend on a set parameters, such as viscosity, dispensing pressure, pushout (early dispensing before cartridge starts to move along the printing path), suckback (sets how much the plunger withdraws at the end of the printing path to stop the extrusion process), nozzle diameters (determines the resolution of the printing process), deposition rate (determines the amount of material deposited for each mm of printing path), print speed (speed at which the cartridge moves along the printing path), path height (distance between consecutive layers) and path space (space between adjacent printing paths) [117, 121].

To accomplish the production of a scaffold through this technique, it is fundamental that a 3D model of the scaffold be obtained. Initially, a 3D model of the scaffold is designed through a

specific software, such as CAD software (e.g. SolidWorks™) or by using real data from patients (computerized tomography (CT) scans). This strategy provides a precise model of the lesion site, enabling the production of a 3D model with the exact size of the defect [116].

Subsequently, the CAD or the scanned model are converted to Standard Tessellation Language (STL) format. This is then loaded onto the Fab@home software, that slices the model into several layers. With the syringe loaded with the solution and equipment properly configured, the scaffold is produced layer-by-layer onto the plotter platform [120, 121]. This feasible, cheap and reproducible technique allows the control over pore size, pore network orientation and morphology when compared to other methods [79, 122]. Also, the templates fabricated by this method present higher mechanical properties which are crucial to fulfill the demands of bone healing applications [79, 122]

1.7. Aims

The overall aim of the present thesis was to design, fabricate and characterize a new 3D cylindrical composite scaffolds functionalized with Graphene Oxide for bone tissue regeneration applications.

The specific objectives of this study were:

- Design of a new 3D template (cylindrical) of scaffolds to be produced, using a computer assisted design software;
- Optimization of the composition of the blends (TCP, AA and GO) to be used in scaffold production;
- Production of the 3D scaffolds loaded/unloaded with GO;
- Evaluation of the mechanical, physicochemical and biological properties of the 3D scaffolds.

Chapter II

2. Materials and methods

2.1. Materials

Alginic Acid (AA), Alizarin Red S (ARS), Amphotericin B, Ascorbic Acid, Calcein powder (MW= 622.53g/mol), Calcium Chloride ($CaCl_2$), Dulbecco's modified Eagle medium: nutrient mixture F12 (DMEM-F12), Gentamicin, Graphite, and Trypsin were bought from Sigma-Aldrich (Sintra, Portugal). 3-(4,5-dimethylthiazol-2-yl)-5-(3-carboxymethoxyphenyl)-2-(4-sulfophenyl)-2H-tetrazolium salt (MTS) was purchased from Promega (Madison, USA). Fetal Bovine Serum (FBS) was acquired from Biotecnómica (São Mamede de Infesta, Portugal). Sodium Hydrogen Carbonate ($NaHCO_3$), Sulfuric Acid (H_2SO_4) and Tricalcium Phosphate (TCP, MW=310.2g/mol) were obtained from Panreac (Barcelona, Spain). Phosphoric Acid (H_3PO_4) was obtained from VWR (Carnaxide, Portugal). Glutaraldehyde 25% (v/v) and Potassium Permanganate ($KMnO_4$) were purchased from Acros Organic (Geel, Belgium). Normal Human Osteoblast (hOB), (406-05f) cryopreserved cells were acquired from Cell Applications, Inc. (San Diego, USA). Wheat germ agglutinin conjugate Alexa® 594 (WGA-594) was bought from Invitrogen (USA). Double deionized and filtered water was obtained using a Milli-Q Advantage A10 ultrapure Water Purification System (resistivity = 18.2 MΩ/cm at 25°C).

2.2. Methods

2.2.1. Layer design and assembly of the scaffold 3D model

Scaffolds were designed through computer assisted design software (SolidWorks™ design software). As represented in Figure 15A, two types of layers were designed, wherein each layer acts as a support for the next layer stacked on top, in order to allow the scaffold to sustain its' structural integrity, while it is being printed.

The final 3D model was assembled by stacking layers α and ß consecutively, layer ß was rotated 45° clockwise upon each cycle. Such strategy was adopted to allow a homogeneous distribution of pores along the scaffolds' structure, resulting in an interconnected pore network aimed at providing adequate porosity while maximizing scaffolds' mechanical strength. The final 3D model is composed of 9 layers with and a diameter of 16mm and height of 10.8mm.

2.2.2. GO synthesis

To obtain Graphene Oxide (GO), graphite oxide was initially synthesized by using a modified version of the improved Hummer's method as we previously described [123]. Shortly, a H_2SO_4/H_3PO_4 solution (9:1 v/v, 67mL) was slowly added to a $KMnO_4$ (3.10g) and graphite (0.51g) mixture in an ice bath. The resulting solution was left to react over a period of 4 days at room temperature (RT), under constant stirring.

Afterwards, the mixture was poured into 67mL of frozen water and H_2O_2 was added until the solution displayed a yellow coloration. The product was then purified through several centrifugations steps (with HCl (3.7%) and water). The resulting material was dialyzed against water for 5 days. Finally, graphite oxide was submitted to sonication cycles, yielding GO (Vibra-Cell VC600-2, Sonic & Materials, CT, USA).

2.2.3. Production of 3D hybrid scaffolds

Scaffolds were fabricated by employing a RP technique, i.e. a Fab@home 3D printer, as previously described by our group [119]. In scaffolds' production, different ratios of TCP/AA (w/w) were used: 60/40, 70/30 and 80/20 respectively. The alginic acid solution (15% (w/v)) was prepared by dissolving the polymer in double deionized and filtered water. Subsequently, TCP powder was added and homogenized to obtain mixtures with different TCP/AA ratios. The resulting TCP/AA polymeric mixtures were homogenized for 30min, using an X10/25 Ultra-turrax (Ystral, Germany). Following, a 5% $CaCl_2$ solution was added to the mixtures, at ratio 1:2 of $CaCl_2$:AA, for allowing the partial cross-linking of AA chains (sodium substitution by calcium). The mixtures of TCP/AA were then loaded into a syringe (10cc Luer Lock) and the scaffolds were then printed.

Thereupon the scaffolds were immersed in a 5% $CaCl_2$ (w/v) solution overnight to achieve full cross-linking of AA chains in the scaffolds' exterior and interior, in order to enhance their structural integrity. Lastly, scaffolds were removed from the $CaCl_2$ solution and air-dried at room temperature (RT), during 48h.

2.2.3.1. Incorporation of GO into the TCP/AA blend

A blend of TCP/AA (60/40 ratio) was chosen as the ideal candidate for GO incorporation, since this is the ratio that better mimics the inorganic/organic ratio found in native bone. Moreover, previous studies demonstrated that 60/40 ratio on composite TCP/AA blends exhibited better mechanical and biological properties [117]. The blend was prepared by adding the TCP powder to the 15% AA solution, followed by the incorporation of GO, until a ratio of 0.5% (w/w), relative to TCP/AA content, was reached. The 60/40_GO blend obtained was then homogenized, loaded

into the Fab@home printer, extruded and crosslinked following the protocol previously described in section 3.2.3.

2.2.4. Scaffolds Physio-Chemical Characterization

2.2.4.1. Attenuated total reflectance—Fourier transform infrared spectroscopy analysis

To characterize the chemical composition of the scaffolds, Attenuated Total Reflectance-Fourier Transform Infrared spectroscopy (ATR-FTIR) was used, following a protocol previously described by our group elsewhere [124]. The acquired spectra represent the average of 128 scans, between 400 and 4000cm^{-1}, with a spectral resolution of 32cm^{-1}. All the samples were crushed into powder, mounted on a diamond window and spectra were recorded with a Nicolet iS10 FTIR spectrophotometer (Thermo Scientific, Waltham, MA, USA). All the components used for scaffold production were also analyzed in a pure state for comparison purposes.

2.2.4.2. Scanning electron microscopy analysis

Scanning electron microscopy (SEM) analysis of the scaffolds was performed in order to characterize the morphology, porosity and surface of the scaffolds. Samples were mounted onto aluminum stubs with araldite glue and sputter-coated with gold, using a Quorum Q150R ES sputter coater (Quorum Technologies, UK). The SEM images were acquired with different magnifications, at an acceleration voltage of 20kV, using a Hitachi S-3400N scanning electron microscope (Hitachi, Japan).

2.2.4.3. Energy dispersive spectroscopic analysis

Energy Dispersive Spectroscopy (EDS) was used to determine the elemental composition of the different materials. To accomplish that, samples were placed onto aluminum stubs, air-dried at RT and analyzed in a XFlash Detector 5010 (Bruker Nano, Germany), according to a protocol previously described elsewhere [117].

2.2.4.4. Characterization of the mechanical properties of the scaffolds

The mechanical properties of scaffolds were evaluated in dry and wet conditions, to mimic the conditions found in the human body. For that, scaffolds were immersed in Simulated Body Fluid (SBF) for 1h. The SBF solution was prepared in accordance with ionic concentrations found in human blood plasma (142.0mM Na^+, 5.0mM K^+, 1.5mM Mg^{2+}, 2.5mM Ca^{2+}, 147.8mM Cl^-, 4.2mM HCO_3^-, 1.0mM HPO_4^{2-}, and 0.5mM SO_4^{2-}) [125]. All samples (n=5) were subjected to compressive assays using Zwick® 1435 Material Prüfung (Ulm, Germany). A crosshead speed of 3mm/min and a load cell of 5kN were used to analyze five specimens of each formulation in each assay. The compressive strength (C_S) was determined using Equation 1 [126].

$$(1)\quad C_s = \frac{F}{w*l}$$

Where *F* is the load at the time of fracture, *w* and *l* represents the width and length of the scaffolds, respectively. Scaffold's Young Modulus (YM) was determined by the stress-strain relation, using Equation 2 [126].

$$(2)\quad YM = \frac{C_s}{H_d}$$

Where C_s represents the scaffolds compressive strength and H_d stands for the height deformation at maximum load.

2.2.4.5. Swelling assays

The swelling capacity of the scaffolds was determined following a protocol previously described in the literature [82]. Briefly, the scaffolds were immersed in Tris buffer solution (1M, pH 7.4) at 37°C, using a stirring speed of 60rpm, during 55h (n=5). At predetermined intervals, samples were withdrawn from solution, and the excess Tris was removed using filter paper. The scaffolds were weighted and re-immersed in the solution. Swelling ratio was calculated through Equation 3.

$$(3)\quad Swelling\ Ratio\ (\%) = (\frac{W_t - W_o}{W_0}) * 100$$

Where W_o and W_t represent the scaffolds' weight at the beginning and end of the assay, respectively.

2.2.4.6. Determination of the water contact angles

The measurement of the water contact angles (WCA) was performed using a OCAH 200 Contact Angle System (DataPhysics Instruments, Germany), operated in a static mode at RT. In this assay, water was used as a reference fluid [119]. For each sample, a water drop (4μL) was placed in different locations on the scaffolds' surface and the contact angle values were determined. The reported contact angles are the average of five measurements.

2.2.4.7. Evaluation of porosity of the scaffolds

Scaffolds' total porosity was determined by a liquid displacement method, according to the procedure previously reported [126]. In brief, scaffolds were weighted, immersed in an absolute ethanol solution (EtOH) for 48h, and weighed again. EtOH was chosen due to its capacity to penetrate inside the scaffolds' structure, without causing neither swelling nor matrix shrinkage as well as avoiding any possible structural changes [127]. The obtained weight values were applied in Equation 4 and scaffolds' porosity was calculated:

$$(4)\quad Porosity\ (\%) = \frac{Wf - Wi}{d_{ethanol} * V_{scaffold}}$$

Where W_f and W_i represent the final and initial scaffold's weight respectively, $d_{ethanol}$ is the ethanol solution density and $V_{scaffold}$ represents the volume of the scaffolds.

2.2.4.8. Characterization of the degradation profile of the scaffolds

Scaffolds' degradation profile was evaluated using a previously described method [128, 129]. Briefly, scaffolds were immersed in DMEM-F12 medium at 37°C under stirring at 60rpm. At predetermined timepoints, the scaffolds were removed from the solution, freeze-dried for 2h and weighted. The degradation percentage at each point was calculated using Equation 5.

$$(5)\quad Weight\ Loss\ (\%) = \left(\frac{W_i - W_f}{W_i}\right) * 100$$

Where W_i corresponds to the initial weight of the sample and W_f to the weight of the scaffold at time t.

2.2.4.9. *In vitro* biomineralization assay

In order to evaluate the bioactivity of the scaffolds, the 3D structures were immersed in a SBF solution (prepared as described in section 3.2.4.4.), at pH 7.4 and incubated at 37°C during 1, 3, 7, 14 and 21 days [130]. At the predetermined intervals, scaffolds were removed from the solution and rinsed with double deionized water to remove excess soluble inorganic ions. The quantification of the calcium and phosphate ions was achieved through EDS analysis. In turn, the deposition and formation of the apatite layers on the surface of the scaffolds was also evaluated by SEM analysis.

2.2.5. Characterization of the biological properties of the scaffolds

2.2.5.1. Evaluation of cell viability and proliferation in the presence of the scaffolds

Cell viability was assessed by growing hOB cells in DMEM-F12, supplemented with 10% heat inactivated FBS, amphotericin B (100µg/mL) and gentamicin (100µg/mL) in 75cm^2 T-flasks. Cells were incubated at 37°C, in 5% CO_2 humidified atmosphere, until cell confluence was attained. Before seeding, scaffolds were cut into smaller pieces, placed in a 96-well plate and sterilized by UV radiation for 1h. Following, a cell density of 10×10^3 per well was used to assess cell viability over 1, 3 and 7 days. The culture medium was replaced every 3 days until the end of the assays. At the end of each timepoint, microscopic images were acquired to assess cell morphology and growth.

The scaffolds' cytotoxic profile was evaluated through a MTS assay, where the cellular metabolism was assessed through metabolic conversion of MTS into water soluble formazan [110]. Shortly, at the predetermined incubation times, medium in each well was replaced by a mixture of 100µL of DMEM-F12 and 20µL of MTS. Then, the plate was incubated for 4h, at 37°C, in 5% CO_2 humidified atmosphere. Finally, the absorbance of the samples was read at 492nm, using a microplate reader (Biorad xMark microplate spectrophotometer). Cells incubated without the materials were used as negative control (K^-), while cells cultured with EtOH (70%) were used as a positive control (K^+).

2.2.5.2. Characterization of cell adhesion on surface of the scaffolds

In order to evaluate the cellular attachment on the surface of the scaffolds, hOB cells were seeded in contact with scaffold samples an incubated during 1, 3 and 7 days [115]. At the predetermined timepoints, samples were washed and fixed with 2.5% (v/v) glutaraldehyde, for 1h. After, samples were dehydrated with growing concentrations of EtOH (50, 60, 70, 80, 90, and 99.9% w/v), and subsequently they were frozen at -80ºC and freeze-dried for 3h. Then,

samples were analyzed through SEM analysis, according to what was described in section 3.2.4.2.

2.2.5.3. Alizarin Red S staining

To quantify and evaluate the scaffolds' ability to promote calcium deposition by hOB cells, an Alizarin Red S (ARS) staining method was conducted following a protocol already optimized by our group [117]. Briefly, cells were seeded (10 x 10^3 cells/well) in contact with scaffolds, in 96-well plates, during 1, 3 and 7 days. After each timepoint, the samples were fixed with 4% (w/v) paraformaldehyde (PFA) solution during 1h. Subsequently, samples were stained with 100µL of ARS (40mM, pH = 4.1-4.3) during 30min, under gentle shaking. Following, the excess of dye was removed from samples by rinsing them 3 times with double deionized and filtered H_2O. Then microscopic images were then acquired to visualize the calcium deposits.

To quantify the calcium deposition, the adsorbed ARS was eluted with 100µL of 10% (v/v) acetic acid solution for 30min, under shaking. Afterwards, samples were vortexed for 30s and the liquid phase was heated to 85°C for 10min. Thereupon, the samples were centrifuged at 14,000g, during 25min, and 100µL of supernatant was transferred to new microtubes. Then the neutralization of the samples was performed by adding 37.5µL of ammonium hydroxide (10% v/v). Finally, the absorbance was read at 405nm using a microplate reader (Biorad xMark microplate spectrophotometer). A calibration curve was performed using solutions with known concentrations of ARS. The experiment was performed for all scaffold formulations, with n = 5.

2.2.5.4. Confocal microscopic analysis

Confocal Laser scanning microscopy (CLSM) was used to characterize cell distribution within scaffolds. In this assay, only the 60/40 and 60/40_GO scaffolds were selected, since these formulations exhibited the better mechanical, physicochemical and biological properties. Here, scaffolds were labelled with Calcein (20µg/mL) and hOB cell membranes were labelled with WGA-Alexa 594® conjugate (5µg/mL), as described in previous works [124, 131]. The cells were seeded in contact with the scaffolds (10 x 10^3 cells/scaffold), in a µ-Slide 8-well Ibidi imaging plates (Ibidi GmbH, Germany). After 24h, imaging experiments were performed with a Zeiss LSM 710 laser scanning confocal microscope (Carl Zeiss AG, Germany), where consecutive z-stacks were acquired. The 3D image reconstruction was performed using Zeiss Zen 2010 software.

2.2.6. Statistical analysis

The statistical analysis of the obtained results was performed using one-way analysis of variance (ANOVA), with the Newman-Keuls post hoc test. A p value lower than 0.05 ($p<0.05$) was considered statistically significant.

Chapter III

3. Results and Discussion

3.1. GO characterization

The successful synthesis of graphite oxide was verified through FTIR and EDS analysis. The FTIR characterization demonstrated that graphite oxide presents several oxygen functional groups, which indicates the successful oxidation of graphite to graphite oxide (Figure 12A) [86, 132, 133]. Moreover, EDS analysis revealed that the graphite oxide presents a carbon:oxygen (C:O) ratio of about 62:38, which is also in agreement with the literature reports [86, 132, 133]. Finally, graphite oxide was exfoliated into a material with nano-sized dimensions, yielding GO (Figure 12B). Taken together, FTIR (Figure 15A) and the DLS (Figure 15B) results confirm the successful synthesis of GO [86, 133, 134].

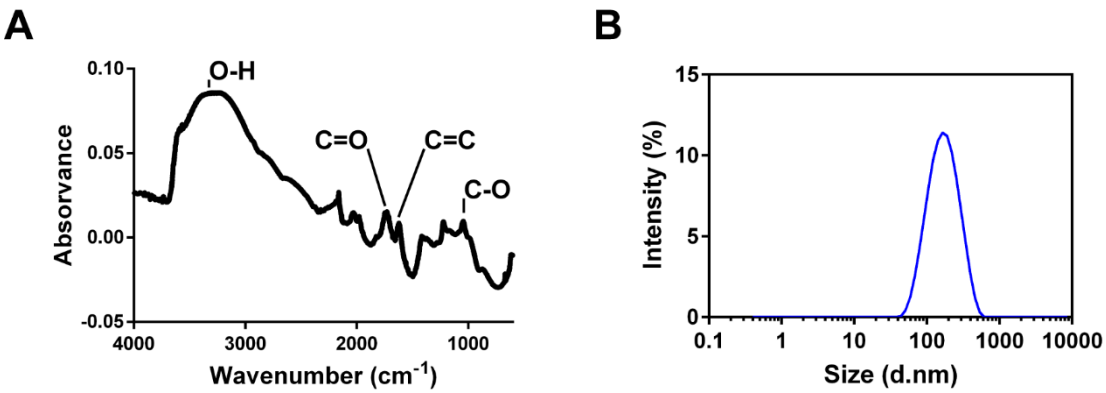

Figure 15. FTIR characterization of graphite oxide (A); DLS size distribution of GO (B).

3.2. Morphological characterization of the scaffolds

Herein, 3D scaffolds were designed using computer assisted design software and produced using a 3D Printing technique. Such approach was used since scaffolds are intended to replicate the structure and composition of the native bone while providing the best compromise between porosity and mechanical resistance. To accomplish that, the 3D scaffolds were produced with a cylindrical shape (as can be seen in Figure 16A), with rather compact periphery to take the load-bearing function similar to the *compacta*, while the interior could be porous like the *spongiosa* of hollow bone. Furthermore, scaffolds need to possess interconnected pores that are fundamental to allow cell in-growth and also provide the required space for neo-vascularization, as described by Leong [135]. TCP and AA were used for scaffolds production, since they are able to mimic the inorganic and organic phases of native bone, respectively. Additionally, GO was incorporated into the scaffolds' composition to improve their mechanical

and biological properties. GO was produced, as described in a previous publication of our group [86].

After scaffolds production, macroscopic images were acquired (see in Figure 16B for further details) to characterize scaffolds shape and pore distribution along their surface. Additionally, it was also noticed that the 60/40_GO scaffold exhibited a dark colour, unlike the white TCP/AA scaffolds. Such change in coloration can be explained by the dark brown colour exhibited by the original GO solution. Moreover, through the analysis of the macroscopic images, it is possible to state that the structure and size of the scaffolds varies according to the scaffolds' ceramic/polymer composition. Here, the TCP content had a direct effect on the scaffolds' dimensions and also on their shrinking, i.e. scaffolds containing the highest percentage of TCP (80/20 scaffold) suffered less shrinkage, since the amount of incompressible ceramic particles limits the shrinking that scaffolds can suffer. Such result was already reported by other researchers [117, 136]. Additionally, the incorporation of the GO into 60/40 formulation did not influence samples shrinking since they presented similar values to that displayed by unmodified scaffolds.

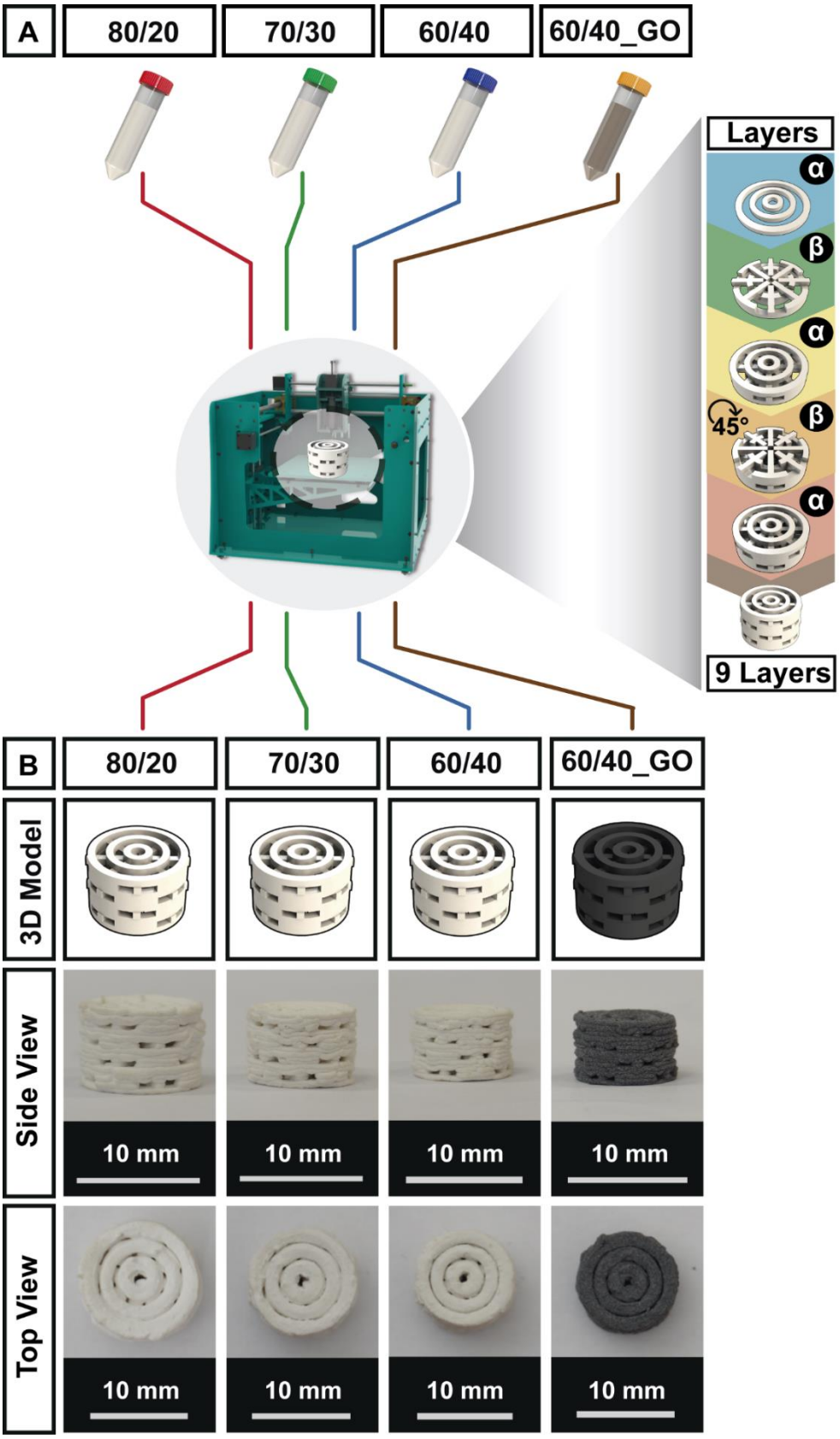

Figure 16. Schematic representation of the process used to produce 3D scaffolds (A); Scaffolds' 3D model and representative macroscopic images of the different produced scaffolds (side and top view) (B).

To further analyze scaffolds' morphology and surface topography, SEM images were acquired at different magnifications. As can be observed in Figure 17, all tested 3D formulations displayed similar surface topography with high roughness and irregularities. A surface with high roughness shows a high number of anchorage points, which encourage protein adsorption, cell adhesion, extracellular matrix components production as well as the metabolism of the human osteoblast cells [137, 138]. Further, rough surfaces also promoted the differentiation of osteoblasts and trigger the bone mineralization process [139]. In comparison to the TCP/AA scaffolds, those containing GO displayed an enhanced roughness. Such is in agreement with data previously published by Leenaerts *et al.*, who reported that substrates coated with GO present an increased surface roughness [140].

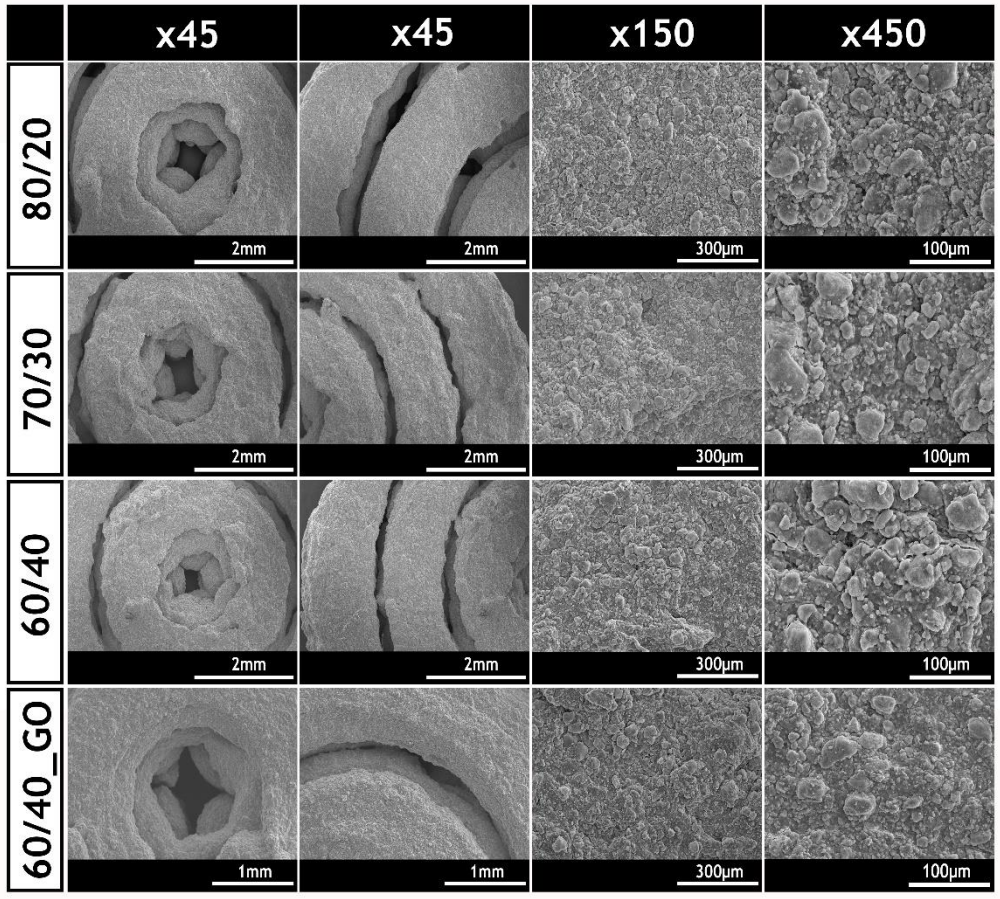

Figure 17. SEM images acquired to characterize the morphology and surface topography of the produced 3D scaffolds.

3.3. Characterization of the physico-chemical properties of the produced scaffolds

3.3.1. ATR-FTIR analysis

ATR-FTIR analysis was used to confirm the composition of the produced 3D scaffolds. As can be observed in Figure 18A, TCP/AA scaffolds displayed an intense absortion peak at 1020 cm^{-1}, which was atributed to P=O strech vibration of inorganic phosphate particles belonging to TCP [115]. Moreover, the obtained spectra also exhibits two major peaks at 1400 and 1600 cm^{-1}, that were assigned to CO_2^- symetric and assymetric stretch, and a peak at 2850-3000 cm^{-1} which is atributed to C-H strech of AA chains [141]. Additionally, the GO containing scaffolds also present a peak between 3000-3600 cm^{-1}, that was attributed to the O-H bonds present in AA [142]. In this way, the characteristic peaks of TCP and AA confirm the presence of these materials in the scaffolds' composition [117].

In Figure 18B is presented the spectra of pure GO and 60/40_GO scaffolds. GO displays peaks at 1049, 1600 and 1720 cm^{-1} corresponding to C-O, C=C and C=O stretch vibrations, respectively. A peak found between 3000-3600 cm^{-1} corresponds to O-H bonds present in the oxygen functional groups of GO nanosheets [86].

Regarding the spectrum obtained for the 60/40_GO, it is possible to observe the presence of the GO, through the visualization of the peaks between 3000-3600 cm^{-1} (belonging to the O-H bonds present in AA and GO) and 1600-1700 cm^{-1} (overlapping of AA C=O stretch and GO C=C stretch) with an increased intensity, despite the low amount of GO added.

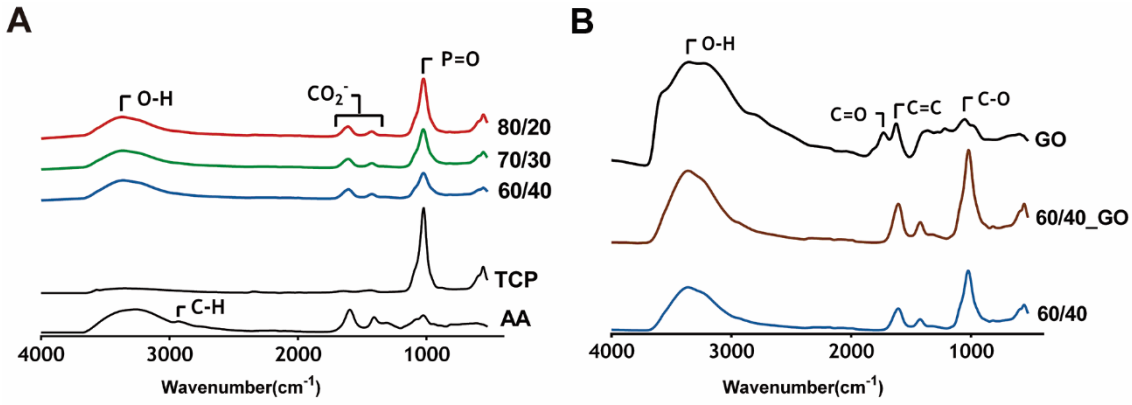

Figure 18. ATR-FTIR analysis of TCP, AA and TCP/AA scaffolds (80/20, 70/30 and 60/40) (A) and GO, 60/40 and 60/40_GO scaffold (B).

3.3.2. Energy dispersive spectroscopy analysis (EDS)

The elemental composition at the surface of the scaffolds was evaluated through EDS analysis. The Ca/P ratios obtained for 80/20, 70/30, 60/40 and 60/40_GO were 2.53 ± 0.41, 2.78 ± 1.15, 3.59 ± 1.36 and 2.98 ± 0.53, respectively. For the 80/20, 70/30 and 60/40 scaffolds, the Ca/P ratio increases when the amount of AA augments, improving the fixation of the calcium ions, at surface of the scaffolds, resulting from the crosslinking process [117]. Notwithstanding, 80/20, 70/30 and 60/40_GO scaffolds presented Ca/P ratios that closely mimic those showed by native trabecular bone tissue (2.33 ± 0.34) [143]. In particular, the 60/40_GO compared to the 60/40 scaffolds show a decreased Ca/P ratio, thereby the incorporation of GO in the 60/40 blend is very important for reproduce the composition of native trabecular bone. The capacity of the GO to promote the adsorption of calcium ions at scaffolds' surface was already described by Xiong *et al*. [90]. This property of GO promotes cell and nutrient infiltration during bone growth, improving the scaffolds' osteoinductivity and osteoconductivity.

3.3.3. Characterization of the mechanical properties of the scaffolds

An ideal scaffold to be used in bone tissue replacement or restoration, needs to fulfill the structural requirements at the lesion site during bone healing, namely the C_s and YM [99]. Herein, scaffolds' C_s and YM were determined using dry and wet samples, as shown in Figure 19.

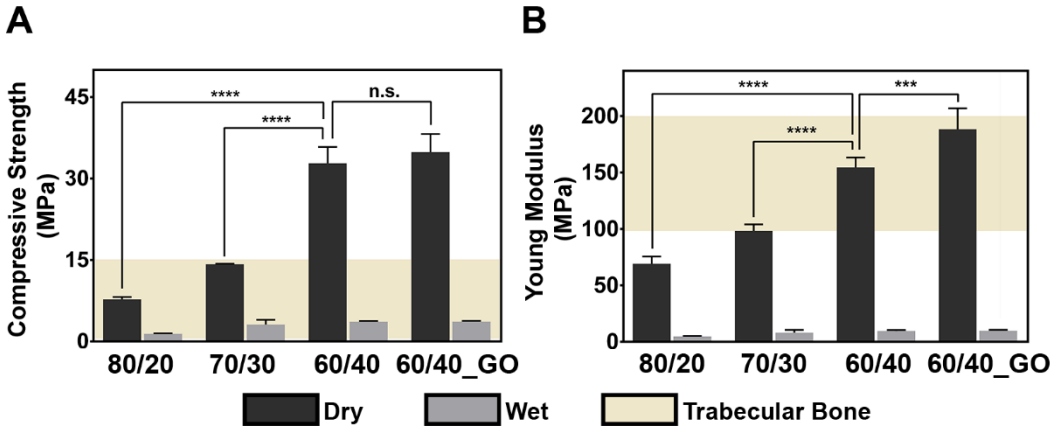

Figure 19. Characterization of the compressive strength (A) and young modulus (B) of the produced 3D scaffolds under dry and wet conditions. Each result is the mean ± standard deviation. The statistical analysis of the results was performed using one-way ANOVA with Newman–Keuls post hoc test (n=5, ***p ≤0.001 and ****p ≤0.0001).

The results obtained revealed that the 60/40 and 60/40_GO scaffolds exhibited the highest C_s, in dry and wet conditions. Such results are in agreement with the data reported in the literature, since 3D constructs with a higher ceramic content (80/20 and 70/30) display an increased brittleness, and consequently, a lower mechanical resistance [144].

On the other hand, the presence of the polymeric component (AA) creates a bone like structure by trapping the TCP particles upon AA crosslinking, conferring to the scaffolds an increased mechanical resistance and elasticity [145]. Although, in wet conditions the compressive strength decreased for all produced scaffolds, the obtained values are similar to that displayed by trabecular bone (0.5-15 MPa), i.e. the produced scaffolds have the required mechanical properties to be applied in non-load bearing sites.

Moreover, the 70/30 and 80/20 scaffolds displayed the lowest YM values (Figure 19B), showing higher elasticity. The 60/40_GO scaffolds displayed an YM of 188.3 ± 18.5MPa, while the 60/40 scaffolds have YM of 154.4 ± 8.7MPa. Despite both formulations had the closest values to YM characteristic of trabecular bone (100-200MPa), the 60/40_GO scaffolds exhibited an viscoelastic behavior closer to that of the native tissue [14]. With this in mind, the 60/40_GO scaffolds present a more adequate mechanical behavior to mimic the trabecular bone tissue [146].

3.3.4. Evaluation of the swelling capacity of the scaffolds

The swelling capability of 3D scaffolds have a strong impact on their mechanical and biological properties. In previous studies it has been shown that scaffolds with an enhanced ability to absorb water from the surrounding environment are prone to have an increased cellular attachment as well as improved protein adsorption [147]. The swelling profiles of the TCP/AA scaffolds revelated that they present a quick swelling in the first minutes, until a plateau is attained after 6h of samples being immersed in Tris buffer (1M, pH 7.4) (Figure 20A). Such swelling behavior was already reported by other authors and such can be explained by the presence of the AA, which is capable of absorbing large quantities of water due to carboxyl and hydroxyl groups present in its structure [82].

The produced 60/40_GO scaffold displayed a swelling profile that only stabilized after 44h of immersion (Figure 20A). In this case, the presence of the GO in the formulation may prevent the initial rapid water absorption seen in the other scaffolds. Here neighboring GO nanosheets could have entrapped polymer and ceramic particles, impairing their interactions with water molecules present in the surrounding medium [90, 148].

In Tissue Engineering, a controlled swelling profile is fundamental since it can impact on the mechanical integrity of the scaffold, triggering a compressive strength on the surrounding

tissue, and ultimately cause pain to the patient [90, 148, 149]. Based on these facts, the 60/40_GO scaffolds presented the most suitable swelling profile for their application in bone tissue engineering.

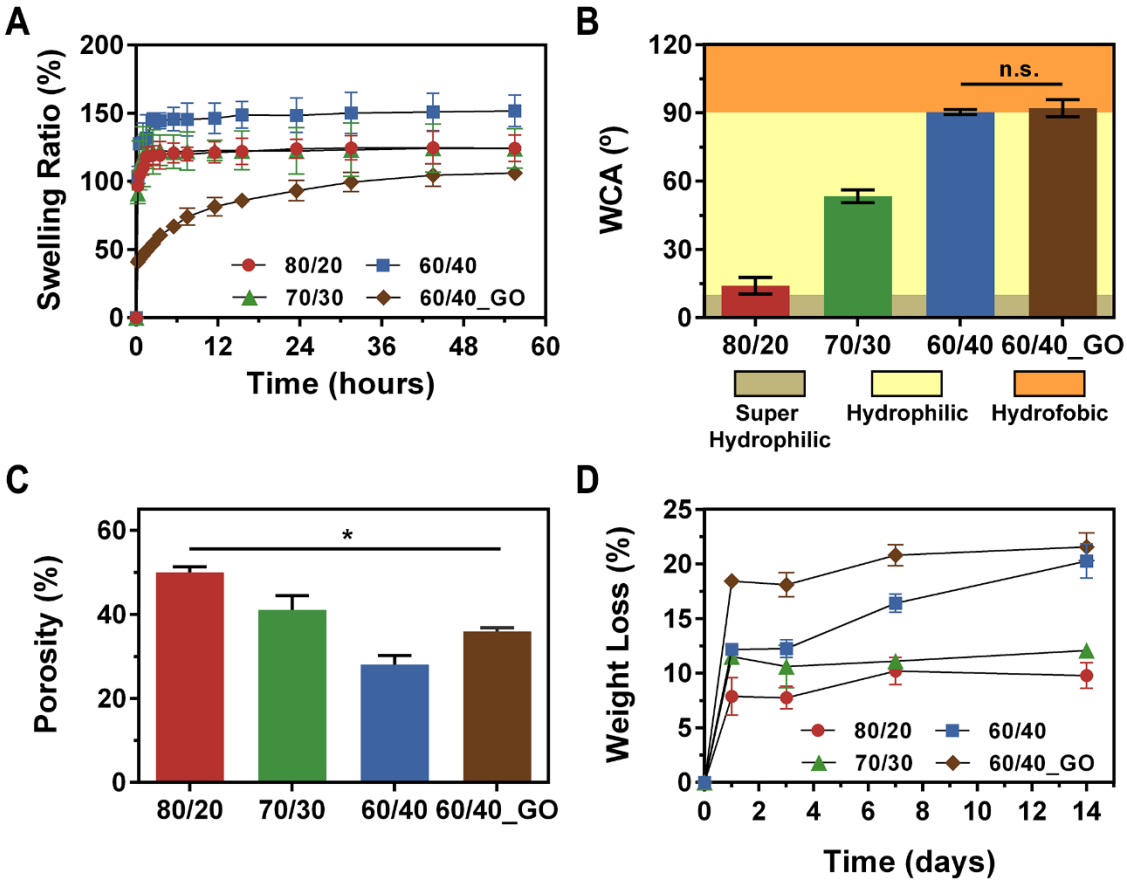

Figure 20. Characterization of scaffolds' swelling profiles (A); determination of water contact angles (WCA) at the surface of the scaffolds (B); evaluation of scaffolds' microporosity (C) and percentage of weight loss of scaffolds along time (D). Each result is the mean ± standard deviation. The statistical analysis of the results was performed using a one-way ANOVA with Newman-Keuls post hoc test (n=5, *p ≤0.05).

3.3.5. Determination of Water Contact Angle

Surface wettability is considered one of the most important properties that affects protein adsorption, platelet adhesion/activation, blood coagulation and cell adhesion. The wettability of the scaffolds may be assessed through the measurement of the water contact angles. Hydrophilic surfaces allow the binding of adhesion molecules that promote cell linkage mediated by membrane receptors, that recognize specific structural motifs available on these molecules. In the literature, a hydrophilic surface is characterized by WCA<90°, whereas a hydrophobic surface displays a WCA>90° [150]. However, highly hydrophilic surfaces (WCA< 10°) can limit/avoid cellular attachment and spreading, since cell adhesion mediating molecules bind weakly to the surface of these materials and they become detached when

several cells interact with them simultaneously [151, 152]. Herein, the 80/20, 70/30, 60/40 and 60/40_GO scaffolds presented WCAs of 14.00 ± 3.63°, 53.32 ± 2.85°, 90.28 ± 1.11° and 92.04 ± 3.77°, respectively (Figure 20B). Such data demonstrates that all 3D formulations possess suitable characteristics for an effective cell adhesion and proliferation.

3.3.6. Evaluation of scaffolds' porosity

A prerequisite of 3D constructs aimed to be used as bone substitutes is that they have an adequate porosity, which is fundamental to grant nutrients, gases and metabolic by-products exchange. The interconnected structure of the pores and their spatial distribution is also essential to promote osteogenesis, cell migration and adhesion onto the scaffolds' surface and interior, as well as to guarantee the mechanical stability of the scaffold [99, 153].

The macroporosity of the scaffolds and the diameter of the macropores were characterized through the SEM images. The macroporosity displayed by the produced scaffolds is in agreement with the total porosity results (Figure 20C). In this regard, the pore size presented by the 70/30 (992μm), 60/40 (755μm) and 60/40_GO (845μm) scaffolds is within the pore size range that is considered to be ideal for nutrient and metabolite mass transfer as well as cell infiltration and bone ingrowth (100-1000μm) (Figure 21) [19].

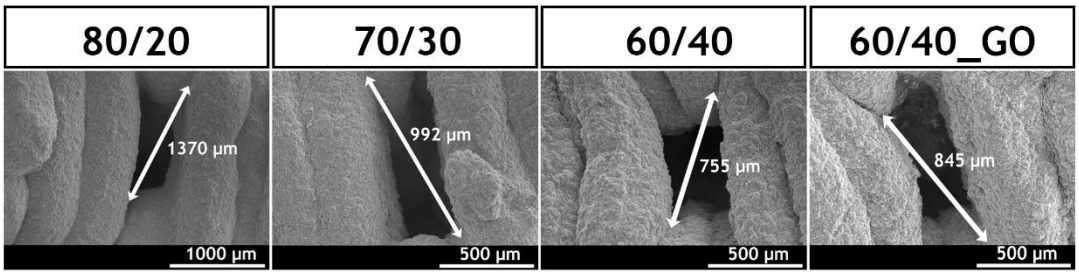

Figure 21. SEM images acquired to determine pore diameters on scaffolds' sides.

Moreover, the total porosity was also characterized and the 80/20 scaffolds, which have the highest TCP content, displayed the highest porosity values (≈ 50%) (Figure 20C). As already reported in literature, scaffolds with a higher ceramic content present more incompressible particles, thus limiting the amount of shrinkage that 3D constructs can suffer, and hence present an increased porosity (Figure 20C) [115].

Furthermore, these results are also in agreement with the mechanical resistance data (Figure 19) since the less resistant TCP/AA scaffolds were those with the higher porosity values. Regarding the native bone tissue, 80/20 scaffolds were the only ones to display a porosity within the range exhibited by the trabecular bone (50-90%), while the 70/30, 60/40 and 60/40_GO formulations exhibited 41%, 28% and 36% porosity values, respectively [154].

In turn, the 60/40_GO scaffolds displayed an increased porosity (≈ 36%), in comparison to the unmodified 60/40 (≈ 28%), which was also accompanied by an increase in their mechanical resistance (higher C_s and YM) (Figure 19B). According to the data available in literature, a balance between the porosity and the density of a scaffold must be established, since a higher density leads to a higher mechanical strength, while a higher porosity provides a favorable biological environment [155]. In this way, even in small loads, GO may be fundamental for the production of 3D constructs that display an improved porosity as well as an appropriate mechanical behaviour [96].

3.3.7. Determination of the degradation profile of the produced scaffolds

After scaffolds implantation within the bone defect, they may suffer some degree of degradation and it is desirable that the released materials do not induce any toxic effect for the host. Additionally, the degradation rates of the scaffolds should ideally meet the bone formation rates [156]. Such is fundamental for the scaffolds to provide the structural integrity to the bone at the lesion site and the adequate framework on which host bone cells can adhere, proliferate and differentiate, while this 3D construct is resorbed by the organism. The results obtained show that scaffolds present a degradation profile that is proportional to the AA content (Figure 19D). Under *in vivo* conditions, AA is enzymatically depolymerized by alginate lyases via a ß-elimination reaction [157]. Furthermore, the depolymerization of AA can also occur due to the gradual replacement of calcium by sodium ions [83]. Additionally, TCP can suffer cell-mediated degradation during the bone resorption process, being solubilized while the new tissue formation occurs [158].

Overall, none of the produced scaffolds lost more than 25% of their initial mass over the period of 14 days, which attests their suitability to act as temporary scaffolds during the bone healing process (Fig. 19D). The 60/40_GO matrices displayed a faster degradation during the first days of incubation which can be correlated with the higher porosity of these scaffolds (Figure 19C). The 60/40_GO scaffolds have an increased surface area that is available to interact with the outside medium and thus trigger a faster degradation in the first minutes of incubation [70, 159]. Nevertheless, the 60/40_GO scaffolds degradation progressively stabilizes at the same values as the ones observed for 60/40 scaffolds. Both types of scaffolds displayed a very similar weight loss after 14 days (Figure 19D).

3.3.8. *In vitro* biomineralization assay

A key factor that is fundamental for the success of any therapeutic approach aimed to be used in bone tissue restoration is the capability of scaffolds' surface to promote its mineralization,

namely through the accumulation of phosphate and calcium ions in the form of hydroxyapatite crystals ($Ca_5(PO_4)_3(OH)$). Such property of the scaffolds reflects their osteoinductivity and osteoconductivity capacities.

In this study, the mineral deposition on scaffolds' surface increased along 21 days when they were incubated in a SBF solution (Figure 22A). Such mineral deposition was characterized by determining the amounts (atomic percentage) of Ca and P present at the surface of all the produced scaffolds (as shown in Figures 22B and 22C). Such results can be explained by the intrinsic capacity of TCP to induce mineralization, leading to an increased integration of the scaffolds within the surrounding bone tissue and consequently enhancing the bone regeneration process [130]. In addition, the presence of the GO in the 60/40_GO scaffolds can improve the nucleation of the minerals due to the higher surface area and charged groups present on the surface of 60/40_GO scaffolds [160].

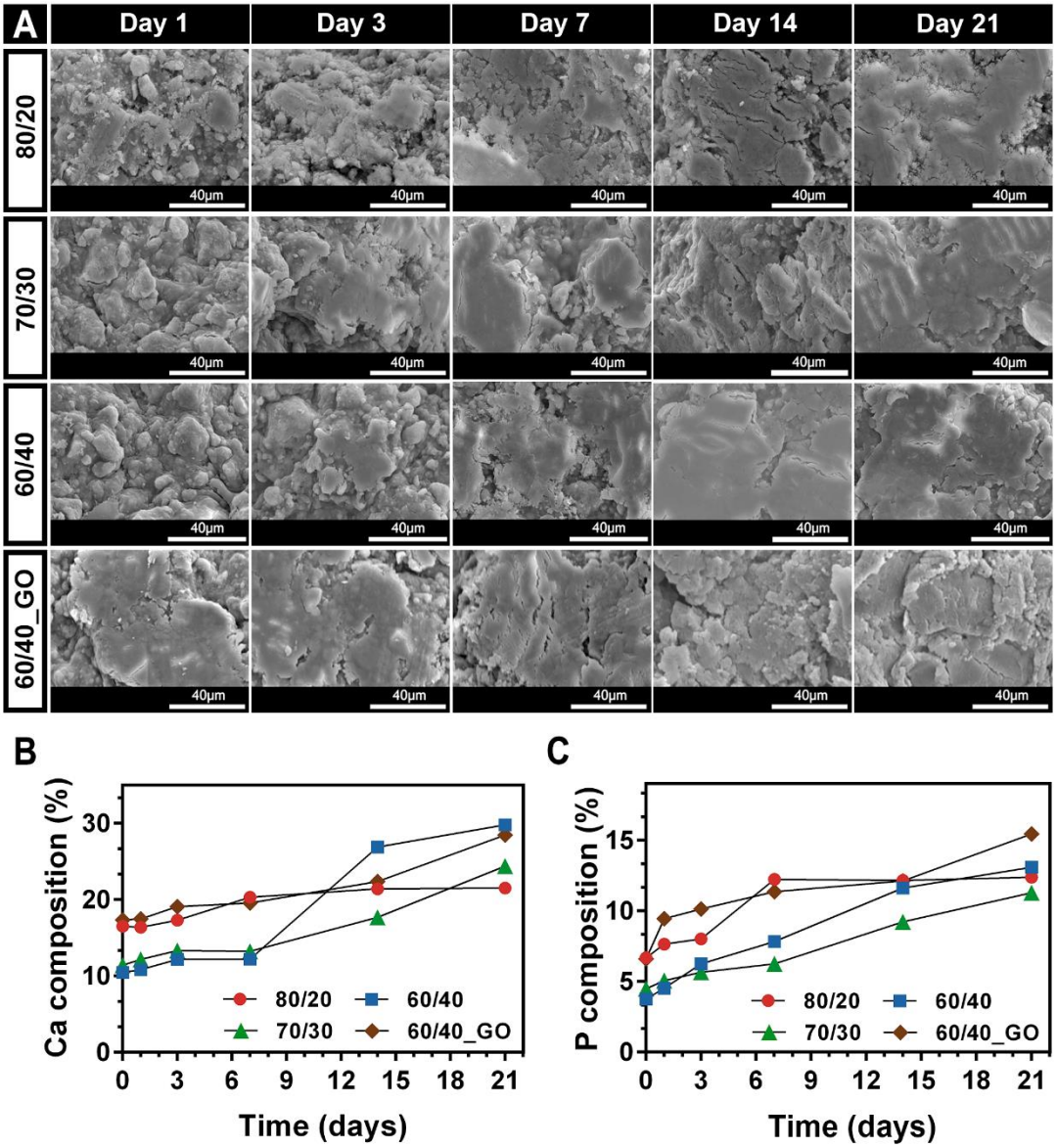

Figure 22. SEM images of the surface of the scaffolds were acquired to characterize the mineral nucleation of the scaffolds' surfaces after their incubation in SBF during 1, 3, 7, 14 and 21 days (A); EDS analysis of calcium (B) and phosphorous (C) atomic percentages at scaffolds' surfaces.

3.4. Characterization of the biological properties of the produced scaffolds

3.4.1. Evaluation of the scaffolds cytotoxic profile

In order to evaluate scaffolds cytocompatibility, *in vitro* studies were carried out by seeding hOB cells in contact with the produced scaffolds. Osteoblast cells were used as model due to their pivotal role on the deposition of new bone ECM as well as on bone tissue remineralization.

The scaffolds biocompatibility was evaluated through a MTS assay after 1, 3 and 7 days of cells be incubated with the different samples (Figure 24A). All the formulations revealed to be biocompatible, i.e., cells displayed a similar metabolic profile to that found in the negative control (Figure 24A). Such data is in accordance with previous results reported by Fradique et. al., who verified that ceramic/polymer composite scaffolds provide an adequate environment for hOB cell adhesion and proliferation [117]. Furthermore, the inclusion of the GO in the 60/40 formulation did not induce any noticeable variation on scaffolds' biocompatibility, as can be verified in the optical microscopic images, where hOB proliferated and remained viable in contact with all scaffolds. Cells exhibit an elongated and flattened morphology, which is similar to that presented by cells in the negative control (Figure 23), thus corroborating the scaffolds' cytocompatibility.

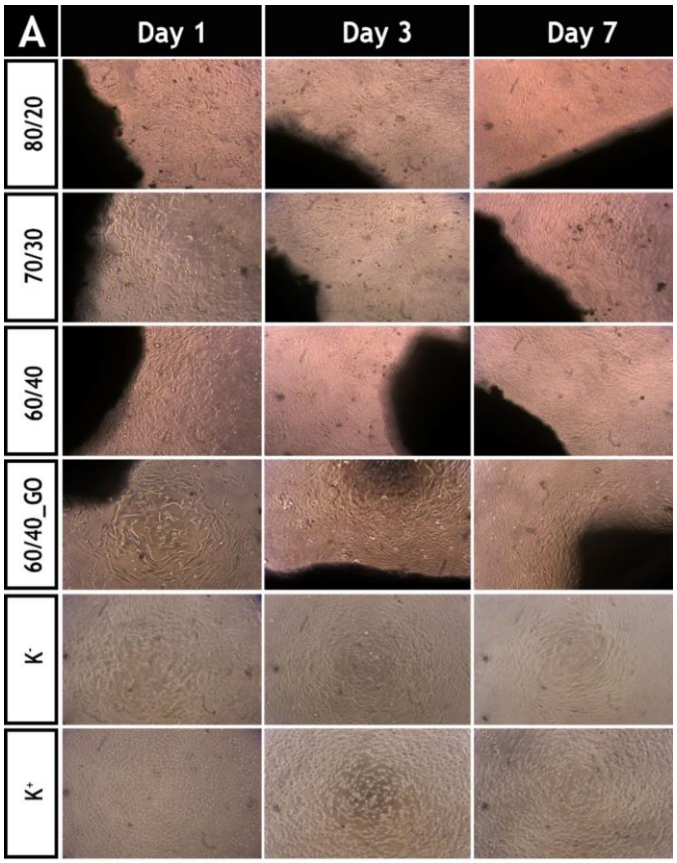

Figure 23. Microscopy images acquired to characterize cell behaviour when in direct contact with scaffolds during 1, 3 and 7 days, negative (K^-) and positive (K^+) controls were also performed.

Despite the fact that GO incorporation into 3D scaffolds, can be associated with some problems related to its toxicity, in the literature it is still widely accepted that GO has a dose and time-sensitive cytotoxicity [161, 162]. Herein, low concentrations of GO were used, and such concentrations did not affect cell viability. When higher concentrations of GO are used a dose-dependent oxidative stress occurs in cells and cell viability decreases [161]. So, we believe that the amount of GO incorporated into the 3D scaffolds was enough to improve the porosity and mechanical properties of these 3D constructs, without impairing cell viability.

Further, the hOB cell attachment onto scaffolds' surface was also evaluated through SEM analysis (Figure 24B). The images show that the cells adhered and spread at the surface of the scaffolds after 1 day (Figure 24B). Moreover, after 7 days a cell layer was observed, demonstrating that the scaffolds are suitable frameworks for cellular attachment, spreading and proliferation, which are crucial features for bone healing applications.

3.4.2. Alizarin Red S staining

An ideal scaffold should promote new bone growth whilst the scaffold is degraded and integrated into the surrounding tissue. During the biodegradation process, the scaffolds release inorganic particles contained in their interior, namely Ca^{2+} which is solubilized and released into the medium. Herein, the mineralization degree of 3D scaffold performed by hOB cells was analyzed by using an ARS staining assay. Optical microscope images of the mineralized matrix at 1, 3 and 7 days are shown in Figure 24C and the calcium content was quantified (Figure 24D). The obtained results revealed that the content of calcium displayed by scaffolds increased after 7 days, which indicates that all the scaffolds promoted osteoblast activity. Interestingly, it was noticed that after 3 days, the 60/40_GO scaffolds displayed the highest concentration of calcium, in comparison to the control. Such data is in agreement with biomineralization assays (Figure 22) and with GOs' ability to induce mineral deposition [92]. In the literature, it has been hypothesized that the surface characteristics of graphene nanomaterials, such as nanotopography, surface stiffness and large absorption capacity influence the calcium deposition, cell proliferation and differentiation, thus contributing for the enhancement of osteogenesis [160]. Moreover, this property of the GO was already demonstrated by Lee et al., who produced the composites of HA composites coated with GO that displayed an increased calcium deposition, and showed a markedly synergetic effect on enhancing the osteogenesis process [163].

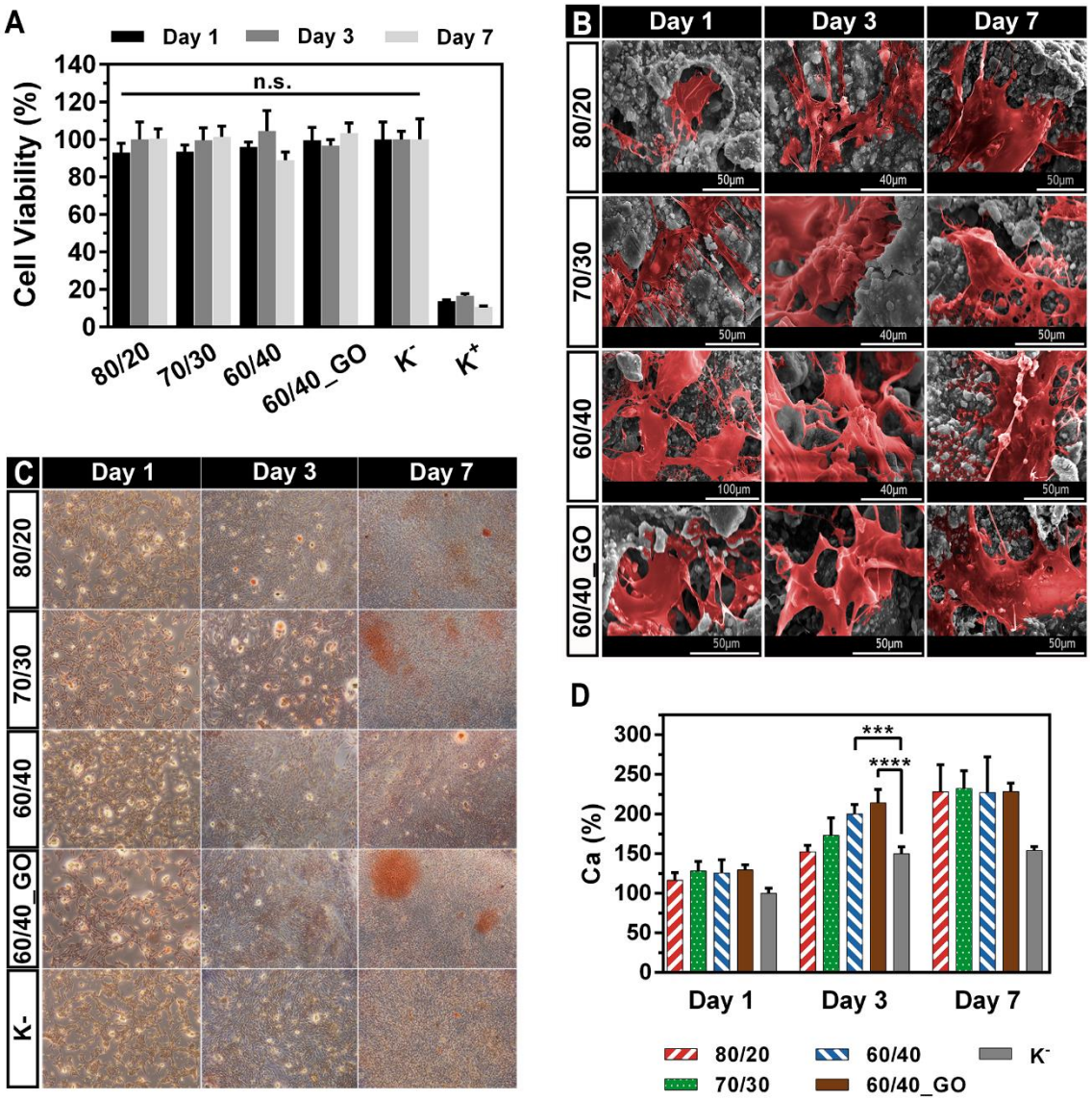

Figure 24. Characterization of the biological performance of the scaffolds. Evaluation of cell viability when cells were seeded in contact with the produced scaffolds after 1, 3 and 7 days. Negative control (K^-) and positive control (K^+) were used for live and dead cells, respectively (A); Each result is the mean ± standard deviation. The statistical analysis of the results was performed using a one-way ANOVA with Newman–Keuls post hoc test (n=5, n.s: no statistically difference). SEM images of hOB cells (pseudo-coloured) seeded on the surface of the scaffolds over a period of 1, 3 and 7 days (B); Evaluation of calcium deposition through Alizarin Red S assay: Optical microscopic images of scaffolds stained with Alizarin Red S (C); and calcium quantification (D) after 1, 3 and 7 days of cells being incubated in the presence of the scaffolds. Each result is the mean ± standard deviation. The statistical analysis of the results was performed using a one-way ANOVA with Newman–Keuls post hoc test (n=5, ***p ≤0.001, ****p≤0.0001).

3.4.3. Confocal laser scanning microscopy analysis

To further characterize the cell internalization and proliferation inside of the scaffolds, an CLSM analysis was performed. The 60/40 and 60/40_GO scaffold formulations were selected for this analysis based on the previously achieved results. The scaffolds were stained with Calcein and cells' cytoskeletons were labelled with WGA-Alexa 594® conjugate. The scaffolds'

structures were characterized as seen in Figures 25A and 25B. Moreover, the 3D reconstructions of the samples presented in Figures 25C and 25D show that osteoblasts adhered and proliferated in contact with the 3D scaffolds, evidencing the biocompatibility and suitable physicochemical properties of the produced scaffolds. Further, the analysis of the orthogonal slices (Figures 25E and 25F) show that osteoblasts start to migrate within the scaffolds, after 24h of incubation. The cellular migration into the scaffolds' structure encourages the deposition of bone matrix that will ultimately fill the lesion with new bone, while the scaffold is biodegraded at a rate that is compatible with the restoration of the structure and function of the native tissue [124, 164].

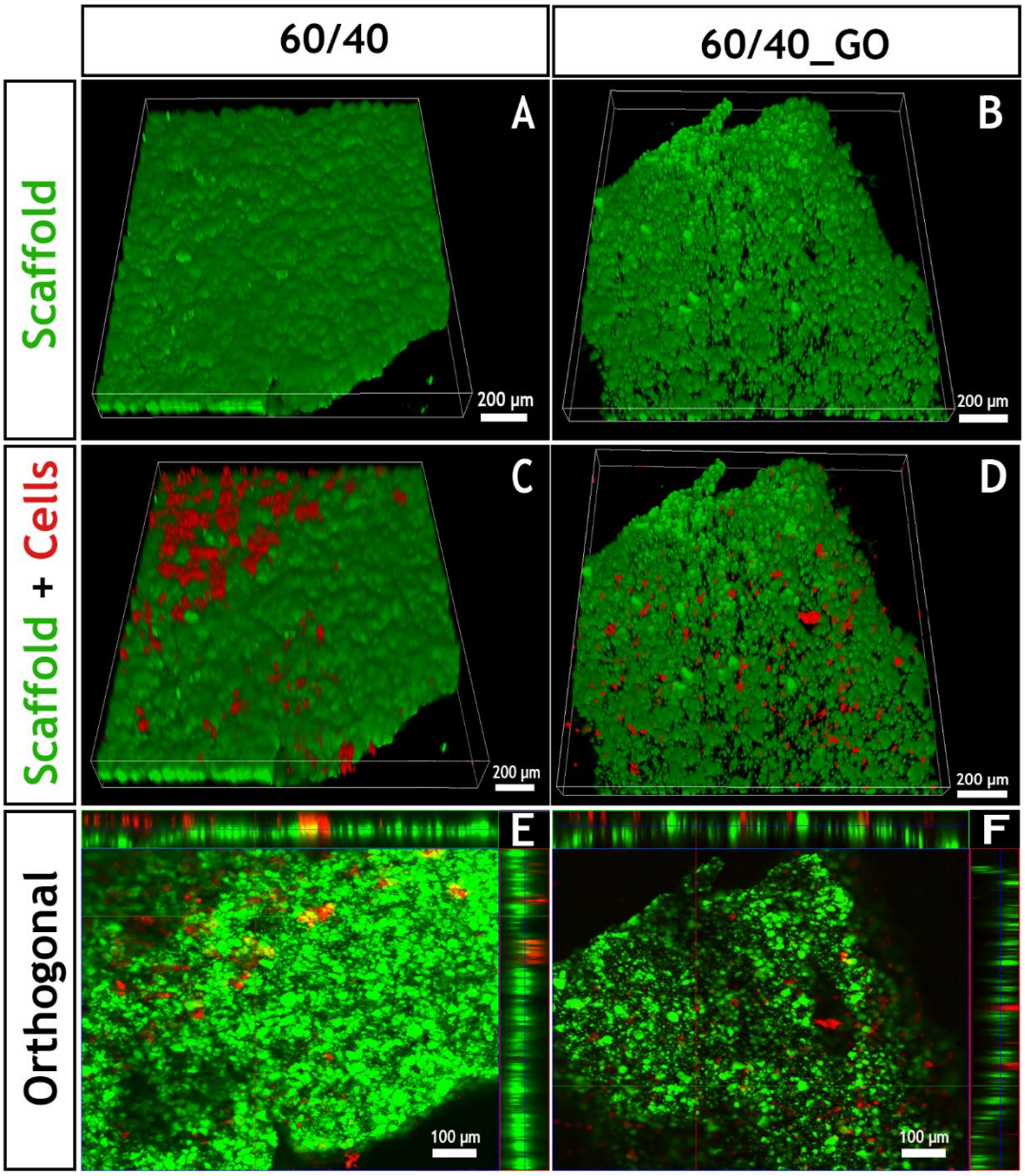

Figure 25. CLSM images acquired to characterize cell internalization within the 60/40 and 60/40_GO scaffolds. 3D reconstruction images (A, B, C and D) and orthogonal projections (E and F) of the cells in contact with the 60/40 and 60/40_GO scaffolds are presented.

Herein, from the best of our knowledge, scaffolds aimed for bone tissue engineering were produced with a bioceramic (TCP) and a natural polymer (AA) using a 3D printing technique. In this way, it was possible to quickly and easily obtain porous biocompatible matrices with a similar architecture to that presented by hollow bones, capable of fine tuning the balance of scaffolds' strength and biological performance. Furthermore, the 60/40_GO scaffolds were produced using only 0.5 % (w/w) GO, which allowed a remarkably improvement of the mechanical resistance and augmented their biomineralization capability of the scaffolds. For instance, in other works, the GO contents required to enhance the mechanical and osteogenic properties was higher (between 1% and 10 % (w/w)) [93, 148]. Overall, in this work the inclusion of GO in the 60/40 formulation led to the production of porous yet stiff scaffolds endowed with the ability to promote osteoblast attachment and mineral nucleation, thus exhibiting the most promising properties for being used in bone healing applications.

Chapter IV

4. Conclusion and Future Perspectives

The demand for new therapeutic options for the treatment of bone injuries has led to the development of various 3D structures in area of Tissue Engineering. These 3D structures aim to mimic bones' nanocomposite structure and composition (organic and inorganic components). Up to now, several techniques have been employed in the production of biocompatible and biodegradable 3D matrices, capable of mimicking the native bones' properties. Among these techniques, RP based methodologies allow the precise control over scaffold architecture, i.e., enable the creation of complex, porous and biodegradable structures. In the present study, a new cylindrical CAD model was created and a TCP/AA biocomposite was extruded with a Fab@home 3D-plotter. Different ratios of TCP/AA were used and GO was incorporated into 3D hybrid scaffolds to enhance scaffolds' mechanical behaviour and their biological properties. Regarding the mechanical performance, the incorporation of the GO into TCP/AA scaffolds increased the compressive strength and young modulus values, making the mechanical properties exhibited by the 60/40_GO scaffolds very similar to that displayed by native bone. Furthermore, the biocompatibility of the TCP/AA and TCP/AA_GO scaffolds was evaluated, demonstrating their non-toxic character for human osteoblast cells, for 7 days. Notwithstanding, GO bearing scaffolds were also able to promote the formation of calcium and phosphate deposits at the surface of the scaffolds.

In addition, the presence of the GO in the scaffolds, even in low concentrations, had a noticeable effect on mineral deposition at the surface of the scaffolds, enhancing the osteoinductive and osteoconductive potential of these scaffolds. Such properties are fundamental for promoting the biomineralization and osteoblast attachment. Due to these features, we believe that TCP/AA_GO scaffolds possess high potential for bone tissue regeneration applications.

Hereupon, the *in vivo* performance of the 3D hybrid scaffolds will be performed in order to further evaluate the potential of the scaffolds for bone healing applications. In addition, the shape of the TCP/AA_GO scaffolds will be optimized to increase their mechanical performance. Moreover, the scaffolds can also be functionalized with bioactive molecules (growth factors, bone morphogenic proteins) to aid the bone healing process and loaded with antimicrobial agents to provide antimicrobial activity, which is crucial for the clinical applications of these scaffolds. Furthermore, the combination of the CAD with RP techniques can allow the design and production of new scaffolds with a high degree of anatomic accuracy that provide a personalized approach to treat osteochondral defects in a simple, quick and cheap manner.

Chapter V

5. References

[1] Salgado AJ, Coutinho OP, Reis RL. Bone tissue engineering: state of the art and future trends. Macromolecular Bioscience 2004;4:743-765.

[2] Kneser U, Schaefer D, Polykandriotis E, Horch R. Tissue engineering of bone: the reconstructive surgeon's point of view. Journal of Cellular and Molecular Medicine 2006;10:7-19.

[3] Porter JR, Ruckh TT, Popat KC. Bone tissue engineering: a review in bone biomimetics and drug delivery strategies. Biotechnology Progress 2009;25:1539-1560.

[4] Doblaré M, Garcıa J, Gómez M. Modelling bone tissue fracture and healing: a review. Engineering Fracture Mechanics 2004;71:1809-1840.

[5] Oryan A, Monazzah S, Bigham-Sadegh A. Bone injury and fracture healing biology. Biomedical and Environmental Sciences 2015;28:57-71.

[6] Hadjidakis DJ, Androulakis II. Bone remodeling. Annals of the New York Academy of Sciences 2006;1092:385-396.

[7] Sommerfeldt D, Rubin C. Biology of bone and how it orchestrates the form and function of the skeleton. European Spine Journal 2001;10:S86-S95.

[8] Olszta MJ, Cheng X, Jee SS, Kumar R, Kim Y-Y, Kaufman MJ, et al. Bone structure and formation: a new perspective. Materials Science and Engineering: R: Reports 2007;58:77-116.

[9] Betts JG, DeSaix P, Johnson E, Korol O, Kruse DH, Poe B, et al. Bone Tissue and the Skeletal System. Anatomy and Physiology OpenStax College; 2013. (accessed on 15/08/2017)

[10] Clarke B. Normal bone anatomy and physiology. Clinical Journal of the American Society of Nephrology 2008;3:S131-S139.

[11] Rho J-Y, Kuhn-Spearing L, Zioupos P. Mechanical properties and the hierarchical structure of bone. Medical Engineering & Physics 1998;20:92-102.

[12] Morrison SJ, Scadden DT. The bone marrow niche for haematopoietic stem cells. Nature 2014;505:327-334.

[13] Ralston SH. Structure and metabolism of bone. Medicine 2005;33:58-60.

[14] Bose S, Roy M, Bandyopadhyay A. Recent advances in bone tissue engineering scaffolds. Trends in Biotechnology 2012;30:546-554.

[15] VanPutte C, Regan, J., Russo, A., Tate, P., Stephens, T., and Seeley, R. Seeley's Anatomy & Physiology: McGraw-Hill Science/Engineering/Math 2013.

[16] Krings A, Rahman S, Huang S, Lu Y, Czernik P, Lecka-Czernik B. Bone marrow fat has brown adipose tissue characteristics, which are attenuated with aging and diabetes. Bone 2012;50:546-552.

[17] Gaalen Sv, Kruyt, M., Meijer, G., Mistry, A., Mikos, A., Meucken, J.v.d., Jansen. J., Groot, K.d., Cancedda, R., Olivo, C., Yaszemski, M., and Dhert, W. . Tissue engineering of bone Tissue Engineering. Burlington Academic Press; 2008. 559-610.

[18] Jayakumar P, Di Silvio L. Osteoblasts in bone tissue engineering. Proceedings of the Institution of Mechanical Engineers, Part H: Journal of Engineering in Medicine 2010;224:1415-1440.

[19] Li X, Wang L, Fan Y, Feng Q, Cui FZ, Watari F. Nanostructured scaffolds for bone tissue engineering. Journal of Biomedical Materials Research Part A 2013;101:2424-2435.

[20] Jang J-H, Castano O, Kim H-W. Electrospun materials as potential platforms for bone tissue engineering. Advanced Drug Delivery Reviews 2009;61:1065-1083.

[21] Downey PA, Siegel MI. Bone biology and the clinical implications for osteoporosis. Physical Therapy 2006;86:77-91.

[22] Sroga GE, Vashishth D. Effects of bone matrix proteins on fracture and fragility in osteoporosis. Current Osteoporosis Reports 2012;10:141-150.

[23] Viguet-Carrin S, Garnero P, Delmas P. The role of collagen in bone strength. Osteoporosis International 2006;17:319-336.

[24] Bao CLM, Teo EY, Chong MS, Liu Y, Choolani M, Chan JK. Advances in bone tissue engineering. Regenerative Medicine and Tissue Engineering: InTech; 2013.

[25] Bailey AJ, Sims TJ, Ebbesen EN, Mansell JP, Thomsen JS, Mosekilde L. Age-related changes in the biochemical properties of human cancellous bone collagen: relationship to bone strength. Calcified Tissue International 1999;65:203-210.

[26] Grynpas M. Age and disease-related changes in the mineral of bone. Calcified Tissue International 1993;53:S57-S64.

[27] Mackie E. Osteoblasts: novel roles in orchestration of skeletal architecture. The International Journal of Biochemistry & Cell Biology 2003;35:1301-1305.

[28] Datta H, Ng W, Walker J, Tuck S, Varanasi S. The cell biology of bone metabolism. Journal of Clinical Pathology 2008;61:577-587.

[29] Meyer U, Meyer T, Handschel J, Wiesmann HP. Fundamentals of tissue engineering and regenerative medicine: Springer Science & Business Media; 2009.

[30] Kular J, Tickner J, Chim SM, Xu J. An overview of the regulation of bone remodelling at the cellular level. Clinical Biochemistry 2012;45:863-873.

[31] Klein-Nulend J, Nijweide PJ, Burger EH. Osteocyte and bone structure. Current Osteoporosis Reports 2003;1:5-10.

[32] Crockett JC, Rogers MJ, Coxon FP, Hocking LJ, Helfrich MH. Bone remodelling at a glance. Journal of Cell Science 2011;124:991-998.

[33] Cohen Jr MM. The new bone biology: pathologic, molecular, and clinical correlates. American Journal of Medical Genetics Part A 2006;140:2646-2706.

[34] Nakamura H. Morphology, function, and differentiation of bone cells. Journal of Hard Tissue Biology 2007;16:15-22.

[35] Raggatt LJ, Partridge NC. Cellular and molecular mechanisms of bone remodeling. Journal of Biological Chemistry 2010;285:25103-25108.

[36] Rucci N. Molecular biology of bone remodelling. Clinical Cases in Mineral and Bone Metabolism 2008;5:49-56.

[37] Boyce BF, Rosenberg E, de Papp AE, Duong LT. The osteoclast, bone remodelling and treatment of metabolic bone disease. European Journal of Clinical Investigation 2012;42:1332-1341.

[38] Danning CL. Structure and Function of the Musculoskeletal System. 2016. 1003. (accessed on 15/08/2017)

[39] Parra-Torres AY, Valdés-Flores M, Orozco L, Velázquez-Cruz R. Molecular aspects of bone remodeling. Topics in Osteoporosis: InTech; 2013.

[40] Matsuo K, Irie N. Osteoclast–osteoblast communication. Archives of Biochemistry and Biophysics 2008;473:201-209.

[41] Sikavitsas VI, Temenoff JS, Mikos AG. Biomaterials and bone mechanotransduction. Biomaterials 2001;22:2581-2593.

[42] Marie PJ. Osteoblast dysfunctions in bone diseases: from cellular and molecular mechanisms to therapeutic strategies. Cellular and Molecular Life Sciences 2015;72:1347-1361.

[43] Lew DP, Waldvogel FA. Osteomyelitis. The Lancet 2004;364:369-379.

[44] Feng X, McDonald JM. Disorders of bone remodeling. Annual Review of Pathology: Mechanisms of Disease 2011;6:121-145.

[45] Svedbom A, Hernlund E, Ivergård M, Compston J, Cooper C, Stenmark J, et al. Osteoporosis in the European Union: a compendium of country-specific reports. Archives of Osteoporosis 2013;8:137.

[46] Shapiro F. Bone and Joint Deformity in Metabolic, Inflammatory, Neoplastic, Infectious, and Hematologic Disorders. Pediatric Orthopedic Deformities: Springer International Publishing; 2016. 411-504.

[47] Teitelbaum SL. Bone resorption by osteoclasts. Science 2000;289:1504-1508.

[48] Rodan GA, Martin TJ. Therapeutic approaches to bone diseases. Science 2000;289:1508-1514.

[49] Whyte MP. Paget's disease of bone. New England Journal of Medicine 2006;355:593-600.

[50] Mast NH, Horwitz D. Osteomyelitis: a review of current literature and concepts. Operative Techniques in Orthopaedics 2002;12:232-241.

[51] Shrivats AR, McDermott MC, Hollinger JO. Bone tissue engineering: state of the union. Drug Discovery Today 2014;19:781-786.

[52] Polo-Corrales L, Latorre-Esteves M, Ramirez-Vick JE. Scaffold design for bone regeneration. Journal of Nanoscience and Nanotechnology 2014;14:15-56.

[53] Damien CJ, Parsons JR. Bone graft and bone graft substitutes: a review of current technology and applications. Journal of Applied Biomaterials 1991;2:187-208.

[54] Woodard JR, Hilldore AJ, Lan SK, Park C, Morgan AW, Eurell JAC, et al. The mechanical properties and osteoconductivity of hydroxyapatite bone scaffolds with multi-scale porosity. Biomaterials 2007;28:45-54.

[55] Costa-Pinto AR, Reis RL, Neves NM. Scaffolds based bone tissue engineering: the role of chitosan. Tissue Engineering Part B: Reviews 2011;17:331-347.

[56] Giannoudis PV, Dinopoulos H, Tsiridis E. Bone substitutes: an update. Injury 2005;36:S20-S27.

[57] Grabowski G, Cornett CA. Bone graft and bone graft substitutes in spine surgery: current concepts and controversies. Journal of the American Academy of Orthopaedic Surgeons 2013;21:51-60.

[58] Liu X, Ma PX. Polymeric Scaffolds for Bone Tissue Engineering. Annals of Biomedical Engineering 2004;32:477-486.

[59] Fröhlich M, Grayson WL, Marolt D, Gimble JM, Kregar-Velikonja N, Vunjak-Novakovic G. Bone grafts engineered from human adipose-derived stem cells in perfusion bioreactor culture. Tissue Engineering Part A 2009;16:179-189.

[60] Collins MN, Birkinshaw C. Hyaluronic acid based scaffolds for tissue engineering—A review. Carbohydrate Polymers 2013;92:1262-1279.

[61] Dvir T, Timko BP, Kohane DS, Langer R. Nanotechnological strategies for engineering complex tissues. Nature Nanotechnology 2011;6:13-22.

[62] Malda J, Visser J, Melchels FP, Jüngst T, Hennink WE, Dhert WJ, et al. 25th anniversary article: engineering hydrogels for biofabrication. Advanced Materials 2013;25:5011-5028.

[63] Williams JM, Adewunmi A, Schek RM, Flanagan CL, Krebsbach PH, Feinberg SE, et al. Bone tissue engineering using polycaprolactone scaffolds fabricated via selective laser sintering. Biomaterials 2005;26:4817-4827.

[64] Luo Y, Lode A, Wu C, Chang J, Gelinsky M. Alginate/nanohydroxyapatite scaffolds with designed core/shell structures fabricated by 3D plotting and in situ mineralization for bone tissue engineering. ACS Applied Materials & Interfaces 2015;7:6541-6549.

[65] Zhou X, Zhu W, Nowicki M, Miao S, Cui H, Holmes B, et al. 3D bioprinting a cell-laden bone matrix for breast cancer metastasis study. ACS Applied Materials & Interfaces 2016;8:30017-30026.

[66] Kutikov AB, Gurijala A, Song J. Rapid prototyping amphiphilic polymer/hydroxyapatite composite scaffolds with hydration-induced self-fixation behavior. Tissue Engineering Part C: Methods 2014;21:229-241.

[67] O'brien FJ. Biomaterials & scaffolds for tissue engineering. Materials Today 2011;14:88-95.

[68] Frohlich M, Grayson WL, Wan LQ, Marolt D, Drobnic M, Vunjak-Novakovic G. Tissue engineered bone grafts: biological requirements, tissue culture and clinical relevance. Current Stem Cell Research & Therapy 2008;3:254-264.

[69] Ma PX. Biomimetic materials for tissue engineering. Advanced Drug Delivery Reviews 2008;60:184-198.

[70] Rezwan K, Chen Q, Blaker J, Boccaccini AR. Biodegradable and bioactive porous polymer/inorganic composite scaffolds for bone tissue engineering. Biomaterials 2006;27:3413-3431.

[71] Henkel J, Woodruff MA, Epari DR, Steck R, Glatt V, Dickinson IC, et al. Bone regeneration based on tissue engineering conceptions—a 21st century perspective. Bone Research 2013;1:216-248.

[72] Campoccia D, Montanaro L, Arciola CR. A review of the clinical implications of anti-infective biomaterials and infection-resistant surfaces. Biomaterials 2013;34:8018-8029.

[73] Chiara G, Letizia F, Lorenzo F, Edoardo S, Diego S, Stefano S, et al. Nanostructured biomaterials for tissue engineered bone tissue reconstruction. International Journal of Molecular Sciences 2012;13:737-757.

[74] Awad HA, Wickham MQ, Leddy HA, Gimble JM, Guilak F. Chondrogenic differentiation of adipose-derived adult stem cells in agarose, alginate, and gelatin scaffolds. Biomaterials 2004;25:3211-3222.

[75] Wegst U, Ashby M. The mechanical efficiency of natural materials. Philosophical Magazine 2004;84:2167-2186.

[76] Choi D, Kumta PN. Mechano-chemical synthesis and characterization of nanostructured ß-TCP powder. Materials Science and Engineering: C 2007;27:377-381.

[77] Holzapfel BM, Reichert JC, Schantz J-T, Gbureck U, Rackwitz L, Nöth U, et al. How smart do biomaterials need to be? A translational science and clinical point of view. Advanced Drug Delivery Reviews 2013;65:581-603.

[78] Cai K, Rechtenbach A, Hao J, Bossert J, Jandt KD. Polysaccharide-protein surface modification of titanium via a layer-by-layer technique: characterization and cell behaviour aspects. Biomaterials 2005;26:5960-5971.

[79] Schieker M, Seitz H, Drosse I, Seitz S, Mutschler W. Biomaterials as scaffold for bone tissue engineering. European Journal of Trauma 2006;32:114-124.

[80] Carvalho MP, Costa EC, Miguel SP, Correia IJ. Tumor spheroid assembly on hyaluronic acid-based structures: a review. Carbohydrate Polymers 2016;150:139-148.

[81] Murugan R, Ramakrishna S. Nano-featured scaffolds for tissue engineering: a review of spinning methodologies. Tissue Engineering 2006;12:435-447.

[82] Valente J, Valente T, Alves P, Ferreira P, Silva A, Correia I. Alginate based scaffolds for bone tissue engineering. Materials Science and Engineering: C 2012;32:2596-2603.

[83] Christensen B. Alginates as biomaterials in tissue engineering. Carbohydrate Chemistry: Chemical and Biological Approaches 2011;37:227-258.

[84] Augst AD, Kong HJ, Mooney DJ. Alginate hydrogels as biomaterials. Macromolecular Bioscience 2006;6:623-633.

[85] Holt BD, Arnold AM, Sydlik SA. In It for the Long Haul: The Cytocompatibility of Aged Graphene Oxide and Its Degradation Products. Advanced Healthcare Materials 2016;5:3056-3066.

[86] de Melo-Diogo D, Pais-Silva C, Costa EC, Louro RO, Correia IJ. D-α-tocopheryl polyethylene glycol 1000 succinate functionalized nanographene oxide for cancer therapy. Nanomedicine 2017;12:443-456.

[87] Dreyer DR, Park S, Bielawski CW, Ruoff RS. The chemistry of graphene oxide. Chemical Society Reviews 2010;39:228-240.

[88] Ruan J, Wang X, Yu Z, Wang Z, Xie Q, Zhang D, et al. Enhanced Physiochemical and Mechanical Performance of Chitosan-Grafted Graphene Oxide for Superior Osteoinductivity. Advanced Functional Materials 2016;26:1085-1097.

[89] Matesanz M-C, Vila M, Feito M-J, Linares J, Gonçalves G, Vallet-Regi M, et al. The effects of graphene oxide nanosheets localized on F-actin filaments on cell-cycle alterations. Biomaterials 2013;34:1562-1569.

[90] Xiong G, Luo H, Zuo G, Ren K, Wan Y. Novel porous graphene oxide and hydroxyapatite nanosheets-reinforced sodium alginate hybrid nanocomposites for medical applications. Materials Characterization 2015;107:419-425.

[91] Rosa V, Xie H, Dubey N, Madanagopal TT, Rajan SS, Morin JLP, et al. Graphene oxide-based substrate: physical and surface characterization, cytocompatibility and differentiation potential of dental pulp stem cells. Dental Materials 2016;32:1019-1025.

[92] Chen G-Y, Pang D-P, Hwang S-M, Tuan H-Y, Hu Y-C. A graphene-based platform for induced pluripotent stem cells culture and differentiation. Biomaterials 2012;33:418-427.

[93] Depan D, Pesacreta T, Misra R. The synergistic effect of a hybrid graphene oxide–chitosan system and biomimetic mineralization on osteoblast functions. Biomaterials Science 2014;2:264-274.

[94] Wu C, Xia L, Han P, Xu M, Fang B, Wang J, et al. Graphene-oxide-modified ß-tricalcium phosphate bioceramics stimulate in vitro and in vivo osteogenesis. Carbon 2015;93:116-129.

[95] Li Y, Feng L, Shi X, Wang X, Yang Y, Yang K, et al. Surface Coating-Dependent Cytotoxicity and Degradation of Graphene Derivatives: Towards the Design of Non-Toxic, Degradable Nano-Graphene. Small 2014;10:1544-1554.

[96] Karageorgiou V, Kaplan D. Porosity of 3D biomaterial scaffolds and osteogenesis. Biomaterials 2005;26:5474-5491.

[97] Sears NA, Seshadri DR, Dhavalikar PS, Cosgriff-Hernandez E. A review of three-dimensional printing in tissue engineering. Tissue Engineering Part B: Reviews 2016;22:298-310.

[98] Hutmacher DW, Sittinger M, Risbud MV. Scaffold-based tissue engineering: rationale for computer-aided design and solid free-form fabrication systems. Trends in Biotechnology 2004;22:354-362.

[99] Hollister SJ. Porous scaffold design for tissue engineering. Nature Materials 2005;4:518-524.

[100] Wu Z, Zheng K, Zhang J, Tang T, Guo H, Boccaccini AR, et al. Effects of magnesium silicate on the mechanical properties, biocompatibility, bioactivity, degradability, and osteogenesis of poly (butylene succinate)-based composite scaffolds for bone repair. Journal of Materials Chemistry B 2016;4:7974-7988.

[101] Kim S-S, Park MS, Jeon O, Choi CY, Kim B-S. Poly (lactide-co-glycolide)/hydroxyapatite composite scaffolds for bone tissue engineering. Biomaterials 2006;27:1399-1409.

[102] Bastami F, Paknejad Z, Jafari M, Salehi M, Rad MR, Khojasteh A. Fabrication of a three-dimensional ß-tricalcium-phosphate/gelatin containing chitosan-based nanoparticles for sustained release of bone morphogenetic protein-2: Implication for bone tissue engineering. Materials Science and Engineering: C 2017;72:481-491.

[103] Zhou C, Yang K, Wang K, Pei X, Dong Z, Hong Y, et al. Combination of fused deposition modeling and gas foaming technique to fabricated hierarchical macro/microporous polymer scaffolds. Materials & Design 2016;109:415-424.

[104] Badhe RV, Bijukumar D, Chejara DR, Mabrouk M, Choonara YE, Kumar P, et al. A composite chitosan-gelatin bi-layered, biomimetic macroporous scaffold for blood vessel tissue engineering. Carbohydrate Polymers 2017;157:1215-1225.

[105] Kalita H, Pal P, Dhara S, Pathak A. Fabrication and characterization of polyvinyl alcohol/metal (Ca, Mg, Ti) doped zirconium phosphate nanocomposite films for scaffold-guided tissue engineering application. Materials Science and Engineering: C 2017;71:363-371.

[106] Dumont VC, Mansur HS, Mansur AA, Carvalho SM, Capanema NS, Barrioni BR. Glycol chitosan/nanohydroxyapatite biocomposites for potential bone tissue engineering and regenerative medicine. International Journal of Biological Macromolecules 2016;93:1465-1478.

[107] Lu X, Qiu T, Wang X, Zhang M, Gao X, Li R, et al. Preparation of foam-like carbon nanotubes/hydroxyapatite composite scaffolds with superparamagnetic properties. Applied Surface Science 2012;262:227-230.

[108] Ma Z, Xie H, Wang B, Wei X, Zhao D. A novel Tantalum coating on porous SiC used for bone filling material. Materials Letters 2016;179:166-169.

[109] Shen F, Cui YL, Yang LF, Yao KD, Dong XH, Jia WY, et al. A study on the fabrication of porous chitosan/gelatin network scaffold for tissue engineering. Polymer International 2000;49:1596-1599.

[110] Serra I, Fradique R, Vallejo M, Correia T, Miguel S, Correia I. Production and characterization of chitosan/gelatin/β-TCP scaffolds for improved bone tissue regeneration. Materials Science and Engineering: C 2015;55:592-604.

[111] An J, Teoh JEM, Suntornnond R, Chua CK. Design and 3D printing of scaffolds and tissues. Engineering 2015;1:261-268.

[112] Peltola SM, Melchels FP, Grijpma DW, Kellomäki M. A review of rapid prototyping techniques for tissue engineering purposes. Annals of Medicine 2008;40:268-280.

[113] Brunello G, Sivolella S, Meneghello R, Ferroni L, Gardin C, Piattelli A, et al. Powder-based 3D printing for bone tissue engineering. Biotechnology Advances 2016;34:740-753.

[114] Martínez-Vázquez FJ, Perera FH, Miranda P, Pajares A, Guiberteau F. Improving the compressive strength of bioceramic robocast scaffolds by polymer infiltration. Acta Biomaterialia 2010;6:4361-4368.

[115] Santos CF, Silva AP, Lopes L, Pires I, Correia IJ. Design and production of sintered β-tricalcium phosphate 3D scaffolds for bone tissue regeneration. Materials Science and Engineering: C 2012;32:1293-1298.

[116] Hockaday L, Kang K, Colangelo N, Cheung P, Duan B, Malone E, et al. Rapid 3D printing of anatomically accurate and mechanically heterogeneous aortic valve hydrogel scaffolds. Biofabrication 2012;4:035005.

[117] Fradique R, Correia T, Miguel S, De Sa K, Figueira D, Mendonça A, et al. Production of new 3D scaffolds for bone tissue regeneration by rapid prototyping. Journal of Materials Science: Materials in Medicine 2016;27:69.

[118] Cohen DL, Lipton JI, Bonassar LJ, Lipson H. Additive manufacturing for in situ repair of osteochondral defects. Biofabrication 2010;2:035004.

[119] Diogo G, Gaspar V, Serra I, Fradique R, Correia I. Manufacture of β-TCP/alginate scaffolds through a Fab@home model for application in bone tissue engineering. Biofabrication 2014;6:025001.

[120] Malone E, Lipson H. Fab@ Home: the personal desktop fabricator kit. Rapid Prototyping Journal 2007;13:245-255.

[121] Kang K, Hockaday L, Butcher J. Quantitative optimization of solid freeform deposition of aqueous hydrogels. Biofabrication 2013;5:035001.

[122] Cox SC, Thornby JA, Gibbons GJ, Williams MA, Mallick KK. 3D printing of porous hydroxyapatite scaffolds intended for use in bone tissue engineering applications. Materials Science and Engineering: C 2015;47:237-247.

[123] de Melo-Diogo D, Pais-Silva C, Dias DR, Moreira AF, Correia IJ. Strategies to improve cancer photothermal therapy mediated by nanomaterials. Advanced Healthcare Materials 2017;6.

[124] Correia TR, Figueira DR, de Sa KD, Miguel SP, Fradique RG, Mendonca AG, et al. 3D Printed scaffolds with bactericidal activity aimed for bone tissue regeneration. International Journal of Biological Macromolecules 2016;93:1432-1445.

[125] Jalota S, Bhaduri SB, Tas AC. Using a synthetic body fluid (SBF) solution of 27 mM HCO 3− to make bone substitutes more osteointegrative. Materials Science and Engineering: C 2008;28:129-140.

[126] Torres A, Gaspar V, Serra I, Diogo G, Fradique R, Silva A, et al. Bioactive polymeric–ceramic hybrid 3D scaffold for application in bone tissue regeneration. Materials Science and Engineering: C 2013;33:4460-4469.

[127] Jiankang H, Dichen L, Yaxiong L, Bo Y, Bingheng L, Qin L. Fabrication and characterization of chitosan/gelatin porous scaffolds with predefined internal microstructures. Polymer 2007;48:4578-4588.

[128] Jeong SI, Jeon O, Krebs MD, Hill MC, Alsberg E. Biodegradable photo-crosslinked alginate nanofibre scaffolds with tuneable physical properties, cell adhesivity and growth factor release. European Cells & Materials 2012;24:331-343.

[129] Freed LE, Vunjak-Novakovic G, Biron RJ, Eagles DB, Lesnoy DC, Barlow SK, et al. Biodegradable polymer scaffolds for tissue engineering. Nature Biotechnology 1994;12:689-693.

[130] Kokubo T, Takadama H. How useful is SBF in predicting in vivo bone bioactivity? Biomaterials 2006;27:2907-2915.

[131] Miguel SP, Ribeiro MP, Coutinho P, Correia IJ. Electrospun Polycaprolactone/Aloe Vera_Chitosan Nanofibrous Asymmetric Membranes Aimed for Wound Healing Applications. Polymers 2017;9:183.

[132] Marcano DC, Kosynkin DV, Berlin JM, Sinitskii A, Sun Z, Slesarev A, et al. Improved synthesis of graphene oxide. ACS Nano 2010;4:4806-4814.

[133] Huang N, Lim H, Chia CH, Yarmo MA, Muhamad M. Simple room-temperature preparation of high-yield large-area graphene oxide. International Journal of Nanomedicine 2011;6:3443-3448.

[134] Neto S, Melo-Diogo D, Correia I, Paquete C, Louro R. Characterization of OmcA Mutants from Shewanella oneidensis MR-1 to Investigate the Molecular Mechanisms Underpinning Electron Transfer Across the Microbe-Electrode Interface. Fuel Cells 2017.

[135] Leong K, Cheah C, Chua C. Solid freeform fabrication of three-dimensional scaffolds for engineering replacement tissues and organs. Biomaterials 2003;24:2363-2378.

[136] Rassis D, Saguy I, Nussinovitch A. Collapse, shrinkage and structural changes in dried alginate gels containing fillers. Food Hydrocolloids 2002;16:139-151.

[137] Rechendorff K, Hovgaard MB, Foss M, Zhdanov V, Besenbacher F. Enhancement of protein adsorption induced by surface roughness. Langmuir 2006;22:10885-10888.

[138] Deligianni DD, Katsala ND, Koutsoukos PG, Missirlis YF. Effect of surface roughness of hydroxyapatite on human bone marrow cell adhesion, proliferation, differentiation and detachment strength. Biomaterials 2000;22:87-96.

[139] Dos Santos E, Farina M, Soares G, Anselme K. Chemical and topographical influence of hydroxyapatite and β-tricalcium phosphate surfaces on human osteoblastic cell behavior. Journal of Biomedical Materials Research Part A 2009;89:510-520.

[140] Shanmugharaj A, Yoon J, Yang W, Ryu SH. Synthesis, characterization, and surface wettability properties of amine functionalized graphene oxide films with varying amine chain lengths. Journal of Colloid and Interface Science 2013;401:148-154.

[141] Lawrie G, Keen I, Drew B, Chandler-Temple A, Rintoul L, Fredericks P, et al. Interactions between alginate and chitosan biopolymers characterized using FTIR and XPS. Biomacromolecules 2007;8:2533-2541.

[142] Daemi H, Barikani M. Synthesis and characterization of calcium alginate nanoparticles, sodium homopolymannuronate salt and its calcium nanoparticles. Scientia Iranica 2012;19:2023-2028.

[143] Tzaphlidou M, Zaichick V. Calcium, phosphorus, calcium-phosphorus ratio in rib bone of healthy humans. Biological Trace Element Research 2003;93:63-74.

[144] Wei G, Ma PX. Structure and properties of nano-hydroxyapatite/polymer composite scaffolds for bone tissue engineering. Biomaterials 2004;25:4749-4757.

[145] Román J, Cabanas M, Pena J, Doadrio J, Vallet-Regí M. An optimized β-tricalcium phosphate and agarose scaffold fabrication technique. Journal of Biomedical Materials Research Part A 2008;84:99-107.

[146] Oftadeh R, Perez-Viloria M, Villa-Camacho JC, Vaziri A, Nazarian A. Biomechanics and mechanobiology of trabecular bone: a review. Journal of Biomechanical Engineering 2015;137:010802.

[147] Tam SK, Dusseault J, Bilodeau S, Langlois G, Hallé JP, Yahia LH. Factors influencing alginate gel biocompatibility. Journal of Biomedical Materials Research Part A 2011;98:40-52.

[148] Belay M, Nagarale RK, Verma V. Preparation and characterization of graphene-agar and graphene oxide-agar composites. Journal of Applied Polymer Science 2017;134.

[149] Li Z, Ramay HR, Hauch KD, Xiao D, Zhang M. Chitosan–alginate hybrid scaffolds for bone tissue engineering. Biomaterials 2005;26:3919-3928.

[150] Dowling DP, Miller IS, Ardhaoui M, Gallagher WM. Effect of surface wettability and topography on the adhesion of osteosarcoma cells on plasma-modified polystyrene. Journal of Biomaterials Applications 2011;26:327-347.

[151] Bacakova L, Filova E, Parizek M, Ruml T, Svorcik V. Modulation of cell adhesion, proliferation and differentiation on materials designed for body implants. Biotechnology Advances 2011;29:739-767.

[152] Oliveira SM, Alves NM, Mano JF. Cell interactions with superhydrophilic and superhydrophobic surfaces. Journal of Adhesion Science and Technology 2014;28:843-863.

[153] Moroni L, De Wijn J, Van Blitterswijk C. 3D fiber-deposited scaffolds for tissue engineering: influence of pores geometry and architecture on dynamic mechanical properties. Biomaterials 2006;27:974-985.

[154] Renders G, Mulder L, Van Ruijven L, Van Eijden T. Porosity of human mandibular condylar bone. Journal of Anatomy 2007;210:239-248.

[155] Ramay HR, Zhang M. Preparation of porous hydroxyapatite scaffolds by combination of the gel-casting and polymer sponge methods. Biomaterials 2003;24:3293-3302.

[156] Dumas JE, Prieto EM, Zienkiewicz KJ, Guda T, Wenke JC, Bible J, et al. Balancing the rates of new bone formation and polymer degradation enhances healing of weight-bearing allograft/polyurethane composites in rabbit femoral defects. Tissue Engineering Part A 2013;20:115-129.

[157] Michaud P, Da Costa A, Courtois B, Courtois J. Polysaccharide lyases: recent developments as biotechnological tools. Critical Reviews in Biotechnology 2003;23:233-266.

[158] Kamitakahara M, Ohtsuki C, Miyazaki T. Behavior of ceramic biomaterials derived from tricalcium phosphate in physiological condition. Journal of Biomaterials Applications 2008;23:197-212.

[159] Walker JM, Bodamer E, Krebs O, Luo Y, Kleinfehn A, Becker ML, et al. Effect of chemical and physical properties on the in vitro degradation of 3D printed high resolution poly (propylene fumarate) scaffolds. Biomacromolecules 2017;18:1419-1425.

[160] Tatavarty R, Ding H, Lu G, Taylor RJ, Bi X. Synergistic acceleration in the osteogenesis of human mesenchymal stem cells by graphene oxide–calcium phosphate nanocomposites. Chemical Communications 2014;50:8484-8487.

[161] Chang Y, Yang S-T, Liu J-H, Dong E, Wang Y, Cao A, et al. In vitro toxicity evaluation of graphene oxide on A549 cells. Toxicology Letters 2011;200:201-210.

[162] Seabra AB, Paula AJ, de Lima R, Alves OL, Dura□n N. Nanotoxicity of graphene and graphene oxide. Chemical Research in Toxicology 2014;27:159-168.

[163] Lee JH, Shin YC, Jin OS, Kang SH, Hwang Y-S, Park J-C, et al. Reduced graphene oxide-coated hydroxyapatite composites stimulate spontaneous osteogenic differentiation of human mesenchymal stem cells. Nanoscale 2015;7:11642-11651.

[164] Liao S, Cui F, Zhu Y. Osteoblasts adherence and migration through three-dimensional porous mineralized collagen based composite: nHAC/PLA. Journal of Bioactive and Compatible Polymers 2004;19:117-130.